Sea level budget in the Bay of Bengal (2002–2014) from GRACE and altimetry

J. Kusche[1], B. Uebbing[1], R. Rietbroek[1], C.K. Shum[23], Z.H. Khan[4]

J. Kusche, Bonn University, Nussallee 17, 53115 Bonn, Germany (kusche@uni-bonn.de)

[1]Bonn University, Bonn, Germany.

[2]Ohio State University, Columbus, U.S.A.

[3]State Key Laboratory of Geodesy and Earth's Dynamics, Institute of Geodesy & Geophysics, CAS, Wuhan, China

[4]Institute for Water Modelling, Dhaka, Bangladesh.

Abstract. Sea level rise is perceived as a major threat to the densely populated coast of the Bay of Bengal. Addressing future rise requires understanding the present-day sea level budget. Using a novel method and data from the Gravity Recovery and Climate Experiment (GRACE) satellite, we partition altimetric sea level rise (6.1mm/a over 2002-2014) into mass and steric components.

We find that current mass trends in the Bay of Bengal are slightly above global mean, while steric trends appear much larger: 2.2 - 3.1mm/a if we disregard a residual required to close the budget, and 4.3 - 4.6mm/a if, as an upper bound, we attribute this residual entirely to steric expansion. Our method differs from published approaches in that it explains altimetry and GRACE data in a least squares inversion, while mass anomalies are parameterized through gravitationally self-consistent fingerprints, and steric expansion through EOFs. We validate our estimates by comparing to Argo and modelling for the Indian Ocean, and by comparing total water storage change (TWSC) for the Ganges and Brahmaputra basins to the conventional GRACE approach. We find good agreement for TWSC, and reasonable agreement for steric heights, depending on the ocean region and Argo product. We ascribe differences to weaknesses of the Argo data, but we also find the inversion to be to some extent sensitive with respect to the EOFs.

Finally, combining our estimates with CMIP5-simulations, we estimate that

Bay of Bengal absolute sea level may rise for additional 37 cm under the RCP4.5 scenario and 40 cm under RCP8.5 until 2050, with respect to 2005.

1. Introduction

Bangladesh is located at the confluence of the Ganges (or Padma), Brahmaputra (or Jamuna), and Meghna rivers, on the northern littoral of the Bay of Bengal. These rivers have formed one of the largest deltaic planes of the world, which, with an area of about 87.000 km^2, provides home to two thirds of Bangladesh's 160 million population. About 6.170 km^2 of the Ganges, Brahmaputra, and Meghna (GBM) delta area are below 2 m elevation (Syvitski et al., 2009), while about 28% of the population lives in the coastal zone (Mohal et al., 2006).

In the Bay of Bengal, the continental shelf is relatively flat and extends up to 200 km in the Western (India) and Eastern (Myanmar) parts, while it is much broader in the Central Bay where it meets the GBM delta. The fan-shaped bay and the delta have experienced devastating storms and surges, including cyclones Bhola in 1970 (resulting in 300.000–500.000 deaths) and Sidr (2007, approximately 4.000 deaths). However, more often (every four or five years) severe monsoonal flooding occurs, inundating more than three-fifths of Bangladesh.

Sea level rise (SLR) is thus perceived as a major threat for the region. SLR will exacerbate the penetration of ocean tides into the river systems and the intrusion of saltwater in the coastal zone, and thus impact fresh water resources and food production. It is linked to increased erosion and changing tidal regimes in channels (Mohal et al., 2006). In addition, SLR is expected to lead to more frequent drainage blocking and river flooding, to more frequent storm surge inundation (Karim and Mimura, 2008), and to an increase in permanently inundated area. As a result, Ericson et al., 2006 estimate that by 2050, 5.5% of the delta area may be lost and 3.4 million of the population may be affected. Mohal et al. (2006) suggest that by 2100 about 4.100 km^2 of the coastal zone will be inundated beyond year 2000 conditions, and that e.g. the Sundarbans world heritage mangrove forest will be lost entirely.

Relative sea level rise (RSLR) represents the combined effect of sea level rise and vertical land subsidence. Past RSLR for the delta has been estimated to 8-18 mm/a (Syvitski et al., 2009) from analysis of several PSMSL tide gauges over 1932-2005, while Ericson et al. (2006) quotes values of up to 25 mm/a. 'Effective' sea level rise ESLR (Ericson et al., 2006), considers, unlike RSLR, the potential for sedimentation: ESLR appears therefore lower than RSLR where sedimentation is present, as in the GBM delta. However, despite the fact that the Ganges and Brahmaputra together carry an estimated sediment load of more than 1000 million tons into Bangladesh (Islam et al., 1999), ESLR may still reach more than 10 mm/a (Ericson et al., 2006). In this paper, we show that absolute sea level rise (ASLR) in the coastal areas of the Bay of Bengal, corrected for glacial isostatic uplift but not for delta subsidence or sedimentation, amounts to 5.5 mm/a from contemporary radar altimeter data (from 2002 to 2014), thus significantly above the global average of about 2.7 mm/a.

However, many studies of future RSLR or ESLR in the GBM delta work with global mean, sometimes across-20th-century, rates and/or projections of uniform SLR, and thus may grossly underestimate the importance of regional variability in the overall assessment (e.g. Ericson et al., 2006, Syvitski et al., 2009, World Bank, 2011). Assessing the impact of rising sea level on coastal regions, inundation, and river network conditions requires assumptions on future coastal–yet–offshore sea level rise to force fine-scale hydrodynamic modelling (Mohal et al., 2006, Karim and Mimura, 2008), and cannot be based on tide gauge analysis only. In order to account for scenarios of anthropogenic modifications (e.g. reservoir construction, accelerated subsidence) and climate change this requires a partitioning of RSLR into vertical land motion, including sedimentation, and ASLR by combined contributions from ocean volume change (i.e. thermosteric and halosteric sea level change) and mass change (i.e. ocean bottom pressure change, resulting from ice sheet and glacier mass imbalance and land-ocean interactions). In addition, since the rate of ASLR in the Bay of Bengal is much higher than the global average, the need for regional projections (Slangen et al., 2012) and thus regional partitioning, is evident.

Vertical land motion is difficult to measure when representative values across the entire delta or its coastline are sought: Alam (1996) estimates that a part of the GBM basin is subsiding at a rate of 22 mm/a, based on well-log data. More recently, Steckler et al. (2010) measured subsidence rates of 12-13 mm/a for Dhaka and Sylhet, using permanent GPS station data. In a literature review of 24 studies, Brown and Nicholls (2015) find a median rate of subsidence of 2.9 mm/a for the GBM delta.

Interannual sea level change in the Bay of Bengal is spatially varying and strongly affected by climate variability (e.g. Singh, 2006, Sreenivas et al., 2012), and therefore challenging to disentangle from isolated (tide gauge) or short (altimetric, Argo) time series.

Llovel et al. (2011) suggest that the biggest contribution to Bay of Bengal ASLR at interannual time scales is volumetric ocean expansion with warming dominating over salinity effects; yet due to sampling problems, missing information about the deep ocean, limited data period and the large variability of the thermosteric component, this may also result in the biggest uncertainty on contemporary and future SLR. Using Argo data, Llovel et al. (2011) find that steric sea level trends in the Indian Ocean, 1.0 mm/a within 0-700 m and 1.2 mm/a within 0-2000 m area-weighted over 2004-2010, are dominated by thermosteric contributions from the upper layer, consistent with ocean modelling and remote-sensing based sea surface temperature. They showed that strong interannual variability in warming of the upper 300 m is strongly correlated with the Indian Ocean Dipole (IOD) index; this also limits the validity of trends. In fact, recent modelling studies (Lee et al., 2015) suggest that Indian Ocean heat content has increased so sharply during 2003-2012 that it now, in the upper 700 m, accounts for more than 70% of the global heat uptake. As a consequence, the Indian Ocean has become increasingly important in modulating global climate variability.

Another source of uncertainty is the contribution of monsoonal winds, river discharge and land water storage change to sea level. It is important to realize that neither of these effects is uniform: wind-driven variability is strong along the eastern and northern coasts and in the western Bay of Bengal (Cheng et al., 2013a), amounting to sea level anomalies at dm level, seasonally varying river discharge affects the circulation in the Bay, albeit much less (amounting to 2-6 cm, Han and Webster, 2002), and land storage change, even if not balanced by discharge, may lead to annual variations in coastal sea level at the cm level (Jensen et al., 2013) through its associated gravitational pull. Wind forcing and river discharge effects on circulation, temperature, salinity and sea level at interannual time scales have been studied through ocean modelling (Han and Webster, 2002, Durand et al., 2011); these studies find interannual variations at much lower level compared to seasonal effects (e.g. less than 1 cm for river discharge), yet this may bias trends derived from short time series.

Zonally alternating winds in the Indian Ocean are known to generate annual equatorial Kelvin waves (Sreenivas et al., 2012, and references therein), and the eastward moving waves reflect energy upon reaching the boundary and propagate along the coast along the Bay of Bengal, while radiating Rossby waves along the eastern rim. Intra- and interannual variability of pathway and intensity of these waves is modulated by IOD and ENSO; this creates interannual non-uniform sea level variability at the dm-level as well as a variability in the depth of the thermocline.

Here, we focus on the various components of contemporary absolute sea level in the Bay of Bengal, along the GBM delta. We investigate a global partitioning of ASLR contributors (Rietbroek et al., 2012, Jensen et al., 2013), based on inverting Jason -1/-2 and GRACE satellite data over the period 2002-2014, along the Bay and confront it with regional and in-situ data including tide gauges. We quantify the contributions of steric sea level from satellite data and compare to various oceanographic data sets. We also assess the contributions of the major ice sheets, land glaciers, and land hydrological storage changes to regional sea level and investigate the consistency of these estimates to regional GRACE maps of mass change.

Our hypothesis is that our inverse framework allows to derive meaningful regional patterns of ASLR, partitioned for the major mass and steric contributions, that may be tested against in-situ and regional data sets. We further hypothesize that these contributions provide a suitable base for deriving regional projections of future ASLR that in turn may provide boundary conditions for fine-scale coastal hydrodynamic modelling and derived coastal impact studies.

This article is organized as follows: In section 2 we describe the global and regional data sets used in this study. While in the appendix we briefly summarize the global inversion method as published in Rietbroek et al. (2012) and Jensen et al. (2013), in section 3 new elements required for regionalization of the method will be summarized. Results on absolute, steric and mass-related contributions to SLR in the Bay of Bengal will be discussed in section 4, where we also will attempt to synthesize projections for the 2050 vs. 2015 framework. The article closes with a set of conclusions.

2. Data

2.1. Global mass and steric fields from GRACE and altimetry

We evaluate monthly global maps of the main sea-level contributors; i.e. steric (sum of thermo- and halosteric) and mass-driven (partitioned into melt sources Greenland, Antarctica, the world's glaciers, and land hydrologic storage change) sea level change. These maps were derived from a global joint inversion of binned Jason-1 and -2 radar along-track altimetry data (downloaded from the RADS data base, Scharroo et al., 2013) and GRACE gravimetry (using full GFZ version RL05a normal equations) over the years 2002-2014 (see appendix). One should note that during GRACE processing, short-term mass change resulting from e.g. wind-driven ocean dynamics is removed from these data, and we restore only the (sometimes artificial) trends from the OMCT background model (Thomas, 2002) to the GRACE data.

Several studies (e.g. Johnson and Chambers, 2013, Dieng et al., 2015) have attempted to close the sea level budget globally or regionally by adding GRACE-derived ocean mass, altimetry and steric grids. This may be viewed as the direct method of partitioning sea level based on observations, and its application has pioneered the identification of present-day drivers of absolute sea level rise. However, in this approach it is required to mask out a coastal strip of 300-500 km width in order to suppress land mass change effects leaking into ocean estimates. We feel this severely limits the application of the direct method to the Bay of Bengal, as land signals are exceptionally strong and removing a coastal strip of 300 km would leave only about half the size of the Bay for averaging.

In the global inversion method (Rietbroek et al., 2012, Jensen et al., 2013, Rietbroek, 2014), patterns of land mass change over ice sheet basins, glacier clusters, and terrestrial water storage are first augmented by their respective sea level fingerprints. These fingerprints model the passive response of the global sea level to each mass forcing pattern individually, consistent in terms of mass conservation, self-gravitation, elastic loading of the ocean bottom (Farrell and Clarke, 1976), and associated changes of Earth rotation. In fact, Vinogradova et al. (2010) have already shown that, on the annual time scale, self-gravitation effects are strong in the Bay of Bengal and suggest they should be visible in observations of ocean mass and bottom pressure.

Furthermore, in the inversion we rely on grids of steric sea level heights but it is important to realize that these are not applied as a direct correction to altimetric sea level. Rather, the leading steric EOFs are computed first and introduced in the inversion as additional ocean patterns, along with the mass fingerprints. Then, all patterns are fitted to match both, GRACE and altimetry data, in a weighted least-squares sense. For the steric patterns this means that we obtain a corrected steric sea level, co-estimated with the mass contributions. No external models for geocenter motion are needed, and no smoothing/decorrelation of GRACE data with the need for rescaling amplitude loss or truncating coastal areas due to leakage is required in the inverse method. Moreover, it allows us to take into account the time-dependent, non-isotropic, latitude-dependent error and correlation pattern of the GRACE data, that are sampled, unlike altimetry, along a drifting orbit that passes through varying repeat regimes over the mission duration.

In order to understand the sensitivity of the inversion method with respect to the (a priori) steric EOF patterns, in this paper we repeat the global inversion/partitioning using gridded data from two alternative sources. First, we derive steric heights from the upper 700m of the Ishii and Kimoto (2009) gridded ocean temperature and salinity data set and, second, from the model outputs of the Finite Element Sea Ice-Ocean Model (FESOM, Timmermann et al., 2009). This leads to two slightly different global inverse solutions for all sea level contributors that we solve for; these will be termed INVERSION01 (using the Ishii and Kimoto EOFs) and INVERSION02 (using the FESOM EOFs). Finally, in order to test the sensitivity towards resolution, we use 100 steric EOFs in INVERSION01 and 200 in INVERSION02, so the latter one has more degrees of freedom.

In the inversion method, after a preliminary fitting of the mass and steric modes as described above, we derive and fit a further set of dominant orthogonal modes from the altimetric residuals. It is important to understand that these residual modes contain all those remaining contributions that cannot be represented along the mass and steric modes used in the first step, and that appear coherent in altimetry. This includes steric signals from the upper ocean that cannot be represented along the leading EOFs of gridded steric data, contributions from deep-ocean warming (Purkey and Johnson, 2010, Dieng et al., 2015), but likely other regional effects including residual ocean dynamics and internal mass redistribution (Johnson and Chambers, 2013) unaccounted for by our base functions. Then, in a second iteration of the global inversion, signals along these leading residual modes from the previous step are co-estimated with all other contributors from the altimetry and GRACE data. For want of a better designation these will be termed as 'residual dynamic signals' here, but care should be exercised in interpreting them, as discussed below.

As the result of this procedure, in both INVERSION01 and INVERSION02 the altimetric time series of absolute sea level (ASLR) is thus explained through (1) mass-related sea level contributions that do account for self-gravitation, rotational forcing, and the present-day elastic loading of the ocean bottom, (2) steric sea level contributions along the spatial modes found in the a priori steric data, (3) residual modes required to explain non-random altimetric sea level variability unexplained by (1) and (2), these residual dynamic signals likely contain residual shallow and deep steric contributions and residual internal ocean mass distribution, and (4) a small noise-type altimetric residual. With the caveat regarding (3) in mind, we will sometimes combine contributions (2) and (3) into the 'total steric contribution'; this is strictly true only if residual mass change is assumed as zero.

In addition, both inversions provide slightly different maps of explained total water storage change (TWSC) over land, from fitting TWSC EOFs derived from a hydrological model (see Section 3.2) to GRACE data while the corresponding sea level change is constrained by altimetry. For the present study, we will focus on the catchment-integrated water mass change in the Ganges and Brahmaputra basins: the obvious reason is that the hydrological regimes of these two rivers are most relevant for GBM delta flooding, while a secondary reason is that the gravitational pull of the basins may be so strong that it might be visible in ocean mass and thus as well in altimetry (Vinogradova et al., 2010, Jensen et al., 2013).

2.2. Regional and in-situ data

2.2.1. Argo-derived ocean temperature and salinity data

Essentially, our global inversion method provides steric sea level change from GRACE and altimetry, mapped onto the leading modes of variability derived from gridded data which may originate (in the version INVERSION01) from Argo temperature and salinity data. Therefore, it makes sense to compare these results to steric sea levels directly obtained from vertically integrating Argo temperature and salinity data.

The first Argo floats have been deployed during the nineties and in 2005 the global coverage reached about 2000 floats (today: > 3500 floats), allowing the derivation of global maps of steric sea level change. Since the floats move freely, affected by currents, sampling is far from uniform. As a consequence, in the Bay of Bengal (for delineation see Section 4.1) the average density of Argo profiles per 1 degree grid cell is quite high compared to the Indian Ocean (see Fig. 1). Yet, at any given month of 2013 there were not more than 40 floats in the Bay, while during 2005 only 10-15 were present.

HERE GOES FIG. 1

Ishii and Kimoto (2009) provide monthly temperature and salinity fields for the global ocean down to 1500 m, derived at 24 levels through Objective Analysis from Argo float and expendable bathythermograph (XBT) data and constraining less well sampled regions to monthly climatological values. These data suggest that thermosteric SLR (3.5 mm/a in 2005-2013) dominates in the Bay of Bengal, whereas halosteric SLR is negative (-0.4 mm/a). While in INVERSION01 we adjusted EOFs of steric height variability derived from these fields to radar altimetry and GRACE, here we use the original data for comparison.

The Indian National Centre for Ocean Information Services (INCOIS) provides monthly gridded $1^\circ \times 1^\circ$ Argo-derived temperature and salinity fields for the Indian Ocean, with 24 vertical levels down to 2000 m, produced by Optimal Interpolation (Udaya Bhaskar et al., 2007) since January, 2004.

Furthermore, we use gridded temperature and salinity fields from the University of Hawaii International Pacific Research Center (IPRC), provided as a monthly global product since January, 2005, with $1^\circ \times 1^\circ$ spatial resolution and covering 27 depth levels down to 2000 m (Hacker et al., 2010). These fields are derived through variational analysis together with absolute dynamic heights, from Argo profile data in combination with velocities.

2.2.2. GRACE-derived mass changes

In the rapidly evolving GRACE literature, at least two different classes of analysis schemes can be distiguished: the 'basin averaging method' that maps GRACE harmonics (or other more localizing spherical basis functions, such as the so-called 'mascons') onto smoothed spatial averages by applying some kind of shape function (underlying the direct budget method), and the inverse methods (as we apply here) where harmonics are 'explained' by forward-modelling and least-squares approaches. These schemes are fundamentally different, and e.g. Jensen et al. (2013) and Chen et al. (2013) have found non-negligible differences in GRACE TWSC results from the same GRACE level-2 data. This is why we chose to compare our inversion results for land water storage variations in the Ganges and Brahmaputra river basins with GRACE-derived mass change, estimated along the more conventional basin averaging approach.

Essentially, for this we use the same GFZ GRACE solutions that are used here in the inversions INVERSION01 and INVERSION02. We apply methods that have been suggested in Wahr et al. (1998), together with anisotropic error decorrelation (Kusche, 2007) and re-scaling of basin averages (Klees et al., 2007). A subtle issue is the common augmentation with certain low-degree terms; in order to be consistent with the global inverse solutions we use the geocenter motion or degree 1 coefficients that the global inversion provides in our basin averaging GRACE solutions.

While we realize that this procedure cannot provide an independent validation of GRACE-based TWSC estimates in the GBM delta, we are confident that it serves as a validation of the inversion methodology, and that the degree of misfit will help in assessing the uncertainty in GRACE-based ocean mass estimates.

3. Methods

3.1. Comparing steric fields

To derive steric height variations $\eta(\lambda, \theta, t)$ from gridded 3D ocean temperature and salinity fields, we use the relation

$$\eta(\lambda, \theta, t) = \int_{-D}^{0} \frac{1}{\rho_0(z)} \left[\rho(\lambda, \theta, z, t) - \overline{\rho}(\lambda, \theta, z)\right] dz \ , \tag{1}$$

where ρ is the density following from the TEOS-10 approach as a function of temperature T and absolute salinity S_A, and ρ_0 is the density of standard sea water at depth z, based on standard ocean salinity (35.16504 psu) and conservative temperature 0° C. In the above, $\overline{\rho}$ is the time-mean of ρ at grid point (λ, θ) and depth z for the considered time period (which may be different for the different temperature and salinity fields). D represents the bottom reference height associated with the temperature and salinity fields.

Eq. (1) has been evaluated step-wise using the Gibbs Seawater (GSW) toolbox (McDougall and Barker, 2011). In step 1, salinity in PSU (practical salinity units) S_P as provided in the gridded fields are transformed to absolute salinities S_A, and ρ_0 is derived for the individual depth levels z. In step 2, we compute the densities ρ, based on measured temperature and derived absolute salinity, for all times and depth levels. Finally, steric height anomalies for each location and time are derived by integrating over all the depth levels.

Steric heights from Eq. (1) can be compared to our global inversion spatially, by computing trend maps, or in the time domain, by comparing the temporal variation of region-averaged anomalies (see Section 4.3).

3.2. Comparing mass fields

Apart from uniform SLR, land water storage mass change in the regions surrounding the Bay of Bengal has a direct effect on sea level due to its gravitational pull. If this effect is in-phase with the global annual cycle of ocean water mass, the hydrologically driven sealevel amplitude is larger compared to the global mean; while when the land water storage is out of phase with the global ocean mass cycle, the hydrologically driven sea-level amplitude is smaller compared to the global mean (Jensen et al., 2013).

In the Jensen et al. (2013) inversion, we forward-modelled the effect of the 33 globally largest hydrological basins on sea level, ignoring land water storage variations not covered by these regions. Here, we extract the 60 most dominant EOF modes found in the global hydrological model WGHM model (Döll et al., 2003) that cover all continental regions except Greenland, and apply the Sea Level Equation (Eq. (A.1), Farrell and Clark, 1976) to them to derive corresponding patterns. For comparison with direct GRACE basin-averaging for the Ganges and Brahmaputra basins from level-2 harmonic coefficients, we then combine the 60 hydrological fingerprints adjusted from GRACE (and altimetry) within our inversion and apply basin averaging in a final step.

As a result, our inversion-based reconstruction of Ganges and Brahmaputra basin-averaged TWSC from the adjusted time evolution $\hat{d}^{(p)}(t)$ of WGHM fingerprints $e^{(p)}(\lambda, \theta)$ (i.e. the x_{hydro} in Jensen et al., 2013, Eq. (2) and (6), and in Eqs. (A.2) and (A.3) in our appendix), reads

$$S^{(i)}(t) = \int_{\Omega_{(i)}} \sum_{p=1}^{P} \hat{d}^{(p)}(t)\ e^{(p)}(\lambda', \theta') \cos\theta' d\lambda' d\theta' \ . \tag{2}$$

Considering the spherical harmonic expansion of the WGHM fingerprints, $e^{(p)}(\lambda, \theta) = \sum\sum e_{nm}^{(p)} Y_{nm}(\lambda, \theta)$, this can be written as

$$S^{(i)}(t) = \sum_{n=1}^{N} \sum_{m=-n}^{n} \theta_{nm}^{(i)} \left(\sum_{p=1}^{P} \hat{d}^{(p)}(t) e_{nm}^{(p)} \right) ,$$

where $\theta_{nm}^{(i)}$ are the spherical harmonic shape coefficients for the Ganges and Brahmaputra basin with area $\Omega_{(i)}$. I.e.,

$$\theta_{nm}^{(i)} = \int_{\Omega_{(i)}} \bar{Y}_{nm}(\lambda', \theta') \cos\theta' d\lambda' d\theta' \ . \tag{3}$$

In contrast, the common basin averaging / rescaling approach applied to timeseries of filtered and destriped GRACE surface mass coefficients $\tilde{v}_{nm}(t)$ is

$$S^{(i)}(t) = \sum_{n=1}^{N} \sum_{m=-n}^{n} \theta_{nm}^{(i)} \frac{1}{f_{(i)}} \tilde{v}_{nm}(t) \tag{4}$$

In the above, $f_{(i)}$ is a rescaling factor that accounts for amplitude loss occuring due to filtering (including spectral truncation) of a 'perfect' signal (Fenoglio-Marc et al., 2012) and that we, here, determined from filtering the WGHM data sets. In what follows, time series from Eq. (4) will be compared to those from Eq. (2), where the $\hat{d}^{(p)}(t)$ have been derived through the inversion, i.e. based on the $\tilde{v}_{nm}(t)$ and the radar altimetry data.

In the conventional GRACE ocean mass approach (Johnson and Chambers, 2013), Eq. (4) is applied to GRACE fields with the respective monthly mean ocean dealiasing products restored, in order to remove dependencies from the GRACE level 1 background processing. However, more critical is that one usually applies Eq. (4) to an ocean basin with 300-500 km coastal stripe excluded, to avoid any contamination with land hydrologic signals.

While the effect of this on the global ocean may be limited, it would pose a major problem in our analysis of the Bay of Bengal, since (1) steric signals appear quite strong in the coastal regions (i.e. up to 500-800 km off the coastline), in particular along the Indian coast, (2) contaminating GBM land water storage changes are very strong, and (3) along the coast, self-attraction and loading effects are strong and likely different from the global mean (Vinogradova et al., 2010). In our inverse approach, removing a coastal stripe is not required since land hydrological signals are explicitly parameterized and solved for simultaneously.

4. Results

4.1. Absolute sea level in the Bay of Bengal

We define the Bay of Bengal according to the International Hydrographic Organization (1953) limited by the the coastlines of Bangladesh and India in the North and West. In the South-West, the boundary follows the eastern coastline of Sri-Lanka and then connects the south tip of Sri-Lanka with the most northern point of Sumatra, Indonesia. In the East, the Bay of Bengal is bounded by the Andaman Islands and by the Andaman Sea, and by the western coastline of Myanmar.

We estimate altimetric ASLR in the Bay of Bengal to 6.1 mm/a for the time period 2002-2014, from binned Jason-1 and -2 sea level anomalies (Tab. 1). After interpolating the geocentric sea level rise from our inversion to the altimetry bins, we derive an average 'explained' rise in the Bay of Bengal of 5.9 mm/a from INVERSION02, and of 5.6 mm/a from INVERSION01. Both results suggest a significantly higher sea level trend in the Bay of Bengal compared to the global mean trend (see Tab. 1), in line with Llovel et al. (2011).

HERE GOES TAB. 1

HERE GOES FIG. 2

Figure 2 first shows the evolution of the Bay of Bengal average sea level, derived from the binned RADS altimetry data (see Figure 3) for each month between 2002 and 2014. The Jason-1 and -2 mission periods, and the shift of the groundtrack of Jason-1 to an interleaved orbit (Fig. 3) after the initial tandem phase, are indicated. Next, the reconstruction of total sea level (i.e. from all contributions that were partitioned in the two inversion runs INVERSION01 and INVERSION02) is compared. We find that in particular sea level explained by INVERSION02 fits remarkably well to altimetry, while INVERSION01 generally follows altimetry well with the exception of few epochs (e.g. mid-2005 or 2012). A possible explanation is the larger degree of freedom within INVERSION02. On the other hand, all fingerprints are defined and fitted globally, while the Bay of Bengal represents only a small portion of the world ocean. Thus, local events (i.e. with regionally confined correlation scales) like additional water masses pushed in and out of the Bay of Bengal by seasonal changing wind fields or extreme events like cyclones might not be captured adequately by the inversion.

HERE GOES FIG. 3

HERE GOES FIG. 4

Mass contributions (i.e. glacier and ice-sheet mass imbalance and terrestrial hydrology) to sea level in the Bay of Bengal, based on INVERSION02, are displayed in Figure 4 (top). Additionally, the – much larger – variability in steric sea level, resulting from changes in temperature and salinity, is shown together with the differences between the two inversions. Figure 4 (bottom) shows the same situation at interannual time scale, i.e. with the strong annual harmonic signal removed and smoothed by a 12-month running mean.

Greenland, Antarctica and land glacier contributions to sea level in the Bay of Bengal show little annual or interannual behavior, with rates above global average for the Greenland contribution and below the global average for the contributions from Antarctica and land glaciers. Antarctica mass imbalance contributes an ASLR of about 0.29 mm/a, while Greenland adds a rate of 0.85 mm/a, and the world's glaciers of about 0.36 mm/a. Not surprisingly, these numbers are hardly affected by the choice of steric fingerprints in the inversion and therefore quite consistent in INVERSION01 and INVERSION02.

HERE GOES TAB. 2

Land water storage variations introduce a strong annual mass signal of about 2 cm amplitude and peaking in boreal summer, as it has been predicted by Vinogradova et al. (2010) and identified for the world ocean (Johnson and Chambers, 2013), albeit at lower amplitude. We find that a gradual increase of water stored on land lowers sea level, with a trend of -0.2 mm/a to -0.3 mm/a. However, this contribution is inferred in the inversion with a lower uncertainty, and it differs to some extent in the two inversion runs. As mentioned before, a further caveat is that in the inversion method, ocean mass changes are explicitly forward modelled as passive response to sea level contributors, while ocean-internal mass redistribution seen by GRACE will end up in the residual dynamics term.

In line with results by Han and Webster (2002), steric sea level anomalies in the Bay of Bengal vary at the dm-level, with an annual amplitude of more than 5 cm and with large interannual variability (Fig. 4, bottom). Combined (steric along a priori modes, and residual dynamic signals, i.e. required to explain altimetry) SLR rates of 4.3 to 4.6 mm/a were derived from the global inversion. These are clearly the largest, but also the most uncertain contributions to the total sea level. Rates from the inversions, with a priori Argo steric patterns (INVERSION01) and ocean model-based patterns (INVERSION02), agree at the level of 0.8 mm/a before and 0.3 mm/a after introducing fingerprints related to residual dynamic signals. Formal 1–sigmas suggest that the steric trends are well-determined at the level of 0.8 mm/a, i.e. considerable uncertainties remain in regional steric partitioning.

Llovel et al. (2011) found a strong correlation between the thermo-steric sea level change in the upper 300 m of the Indian Ocean and the Indian Ocean Dipole (IOD) index. The IOD represents a measure of difference in sea surface temperature between a western Indian Ocean pole (in the Arabian Sea) and an eastern pole (south of Indonesia). Comparison of IOD with the steric sea level change as inferred from INVERSION01 and INVERSION02 according to the processing in Llovel et al. (2011) for the Indian Ocean shows correlations of 0.57 and 0.28, respectively. The lower correlation of INVERSION02 is probably related to the different depth levels (sea surface to sea floor) covered compared to the upper 700[m] of INVERSION01. For the Bay of Bengal we find correlations of -0.19 and -0.38 for INVERSION01 and INVERSION02, respectively, suggesting still a loose coupling. However, it becomes clear that there are distinct steric changes in the Bay of

Bengal which can not be explained by IOD events.

Our inverse method allows us to reconstruct steric sea level from a subset of the spatial modes only that were fitted to the data. We believe that comparing reconstructions with a subset of steric orthogonal modes – i.e. those derived from an ocean model or from Argo data down to some depth – to those that contain in addition (residual) 'deeper' EOF modes or those obtained from altimetric residuals provides clues on the deep ocean contribution to inferred steric sea level. However, as has been mentioned before, the validity of this hypothesis is subject to sampling issues and the unknown nature of the true depth-dependency of temperature and salinity, and the following should be seen as indicative only. With this in mind, we find that a direct comparison of the steric trends derived for the total ocean depth in INVERSION02 (3.1 mm/a, derived using model based EOFs) and for the upper 700 m of the ocean in the INVERSION01 (2.2 mm/a) indicate a significant contribution from the ocean below 700 m of nearly 1 mm/a in the Bay of Bengal (Tab. 2). This is additionally implied by the lower trend of the residual dynamics fingerprints of INVERSION02 (1.5 mm/a), which would not include deep ocean effects (assuming the modes of variability derived from the ocean model are correct), compared to the residual-mode trend from INVERSION01 (2.1 mm/a). Fig. 4 B) reveals that the total steric signal in the Bay of Bengal (including residual modes but with the annual contribution removed) contains strong interannual variability. In fact, we know that local extreme events, such as heavy monsoonal rainfalls during June-October in certain years, are associated with a significant increase in freshwater influx from the GBM system into the Bay of Bengal. While the annual scale of this is 5-10 times compared to the dry season

(Papa et al., 2010), leading to seasonally reduced salinity (Vinayachandran et al., 2013) and an increase in water volume, interannual variability in salinity has been considered as strong north of 10° N, Durand et al. (2011). Yet, Han and Webster (2002) suggest these account only for about 1 cm at interannual time scale. On average for our time frame we find only a slight reduction of discharge (-370 $m^3/s/a$ at Mawa gauge), such that we do not expect interannual monsoon variability to distort trends. Yet, another potential explanation could be that we observe changes in mass from seasonal changing, wind-driven in- and outflux in the Bay of Bengal, in the altimetric residuals and thus in the residual fingerprints.

Following Sreenivas et al. (2012), we compute a monthly climatology of sea level reconstructed from our inversion, including a combination of steric and residual modes, and, for comparison, from Ssalto/Duacs AVISO mean sea level anomalies (MSLA, `http://www.aviso.altimetry.fr/duacs/`). We find the two cycles of upwelling (January-March and August-September) and downwelling (April/May - July and October-December) Kelvin Waves in a combination of steric and residual contributions well defined and in good agreement with AVISO MSLA based results which have been processed according to Sreenivas et al. (2012) for our inversion time period. This result increases our confidence that our inversion is able to reconstruct a meaningful partition of total sea level change; Although, the utilized combination of steric and residual modes is defined globally, the dominant wave patterns in the Bay of Bengal are reconstructed well.

Finally, we compare steric rates within the Bay of Bengal from the two inverse solutions to those from Ishii/Kimoto, IPRC, and INCOIS for the time frame common to all data sets

(2005-2013). We find IPRC and Ishii and Kimoto (2009) at the lower end with 2.8 mm/a and 3.1 mm/a. INVERSION01 (3.7 mm/a) and INCOIS (3.9 mm/a) point to higher rates, while INVERSION02 suggests a total steric rate of even 4.6 mm/a. This range of estimates appears quite disparate, yet one has to recall that Argo based products, in this case, refer to the upper 700 m only, and that the time frame is short (formal errors from time series fitting are at the 1 mm/a level). As was mentioned earlier, it is impossible to provide a corresponding altimetry minus GRACE estimate due to land contamination effects (if we remove a 300 km coastal stripe, almost half of the area of the Bay, altimetry minus GRACE amounts to even 6.6 mm/a following methods described in Johnson and Chambers (2013)).

4.2. Sea level at tide gauges in the Bay of Bengal

Tide gauges (TGs) measure relative sea level at higher temporal resolution compared to altimetry, and much longer time series have been recorded. Although TG data do not directly validate our partitioning in mass and steric contributions, it is interesting to ask how well our Jason-based inversion fits to recorded time series at short and interannual timescales. Following suggestions regarding an early version of this paper, we use PSMSL data (Holgate et al., 2013, PSMSL, 2015) for three gauges (Chennai, Visakhapatnam, Chittagong) whose records cover at least a larger part of the inversion time frame. However, in order to understand spatial sampling effects related to Jason orbits, we also compare to AVISO multi-mission sea level anomalies. In summary, we find good fits at Chittagong and much less agreement for the Indian stations, likely related to track distance and proximity to open ocean. We find our inversion / Jason altimetry in slightly lower agreement with TGs compared to AVISO, as expected.

The Chennai gauge is located at the SE Indian coast (13.1°N, 80.3°E) in between nominal Jason groundtracks 040 and 155, while Visakhapatnam is found at the east Indian coast (17.68°N, 83.28°E) close to groundtracks 116 and 155. Chittagong is situated at west coast of Bangladesh (22.24N, 91.83E) close to groundtrack 053. Monthly averaged PSMSL TG data have been corrected for the inverse barometric effect using monthly ERA-Interim mean sea level pressure fields (Dee et al., 2011). No GNSS-based vertical motion rates are known for these TGs and published PSMSL corrections from GIA-modelling are below 0.35 mm/a, so we decided not to apply any correction for land motion in the following. The TG time series are shown as black lines in figure 5.

As mentioned above, we extend the comparison to AVISO mean sea level anomalies. Since AVISO MSLAs include altimetric data with higher spatial resolution compared to Jason-1/2, we expect this comparison to tell what level of fit can be expected at all between altimetry and TGs. In a first step, all total sea level anomalies from AVISO (resampled to the 0.5 degree inversion grid) and from our inversion within a bounding box of $\pm 2°$ around the TG positions have been averaged to time series that can be compared to the TG data (Fig. 5, purple and green lines). As will be explained below, a second group of time series has then been created where we reject grid points in the box averaging that show poor correlation.

HERE GOES FIG. 5 A straightforward comparison of box-averaged altimetry to gauge-read time series reveals little correlation for Chennai ($R^2_{AVISO} = 0.07$, $R^2_{INV02} = -0.17$)

and Visakhapatnam ($R^2_{AVISO} = 0.25$, $R^2_{INV02} = 0.18$), while at Chittagong gauge data, AVISO, and 'explained' sea level in the inversion show good correspondence ($R^2_{AVISO} = 0.89$, $R^2_{Inv02} = 0.81$). To understand the reason for this behaviour, we then created correlation maps between three TGs and all grid point of the inversion (Fig. 6) and AVISO MSLA (Fig. 7). These maps reveal that for Chennai and Visakhapatnam, correlation to both AVISO and inversion is strong (> 0.5) close to the station and along the continental shelf but drops rapidly for open-ocean nodes. This effect is somewhat stronger for AVISO, since the inversion inherits its spatial resolution from the Jason data, which is lower and sometimes yields undefined pixels close to the coast. For the Chittagong TG (Fig. 6, C and Fig. 7, C), larger areas of strong correlation are clearly related to the larger coastal shelf in the northern Bay of Bengal. Yet, this is not unexpected as our comparison includes the full annual dynamics of sea level in the Bay of Bengal (see e.g. lag-correlation maps in Sreenivas et al., 2012). Thus, the maps explain the weak correlation of $\pm 2°$ box-averaged time series: The Chittagong 'TG box' largely covers the shelf and the average is computed from high–correlation values only, while for Chennai and Visakhapatnam large parts of box are open ocean where significantly weaker or even negative correlations are present.

HERE GOES FIG. 6 HERE GOES FIG. 7 To overcome this situation, we edited the time series from AVISO and inversion by averaging only grid points within the bounding box with correlation > 0.6 (orange and blue in Fig. 5). For Chennai, correlation increases to $R^2_{AVISO} = 0.92$ and $R^2_{INV02} = 0.62$. However, with this modification, only 32% of AVISO and even only 3.5% (just one node) of the ocean grid points passed the threshold, due to lower spatial resolution. At Visakhapatnam, the effect of editing is less (Fig. 5, B) and correlations increased to $R^2_{AVISO} = 0.90$ and $R^2_{INV02} = 0.71$. This gauge is located closer to a Jason groundtrack and we find better agreement between the inversion results and the TG, while these are still somewhat lower compared to AVISO. This is consistent with an observed difference between AVISO and our inversion / Jason 1/2, resulting in only moderate (0.5-0.7) correlation between these two grids in the coastal shelf close to the Chennai and Visakhapatnam, as well as in two small regions in the central Bay of Bengal, whereas in general in the Bay we find correlations of > 0.7. Again, the reason is thought to be related to the lower spatial resolution of Jason and its effect is part of ongoing investigations. Finally, and as expected, for Chittagong (Fig. 5, C) the situation is different and we find nearly the same correlations ($R^2_{AVISO} = 0.89, R^2_{INV02} = 0.83$) for AVISO MSLA and our inversion.

4.3. Steric contributions to sea level in the Bay of Bengal

Over the time period considered, steric sea level is the most dominant contributor to the total sea level change in the Bay of Bengal (Fig. 4). Ocean temperature and salinity experience a strong influence by seasonal phenomena such as the annual monsoon cycle and corresponding changes in freshwater influx into the bay, as well as seasonal changes in temperature. However, these changes are difficult to measure, especially at depth. Large parts of the Indian Ocean and also the Bay of Bengal are deeper than 2000 m and it is unclear what their contribution to the total sea level is. Both, GRACE and altimetry measure depth-integrated effects and we expect our global inversion to provide steric sea level variability relatively free of this limitation. In the following, we will investigate the steric results from our inversion in a broader context and compare them to independent steric fields from Argo data.

HERE GOES FIG. 8

The global inverse solutions that we considered so far involve two systems of base functions for representing steric patterns, the first one either derived from the FESOM ocean model (INVERSION02), or from an upper-ocean ($>$ 700 m) steric Argo data set (INVERSION01), and the second one derived from altimetry residuals with respect to an inversion with these first mentioned set of patterns only. As mentioned before, for INVERSION01, under certain assumptions one may consider heights associated with this second set of base functions containing deep-ocean steric contribution from GRACE and altimetry: (1) In fact, if deep-ocean steric patterns are significant at the altimetric noise level and they appear collinear with upper-ocean ones, then they would rather amplify the first set of modes, while (2) that part of deep ocean warming that is not collinear with the Argo-derived modes will appear in the second set of base functions. As a result, the sum (total steric) of the modes will contain such contributions (if they are significant), but other effects like circulation change or wind-driven mass relocation may be present in the altimetry data and contaminate these results. It is important to understand that the interpretation differs slightly in INVERSION02: Here, the first set of base functions contains modes found in modelled deep-ocean steric expansion, and those modes in real shallow and deep ocean steric variability that cannot be explained by the modelled ones will end up in the second set of base functions. With this caveat, Fig. 8 shows the combined steric effect based on the fingerprints from the FESOM model or the Ishii and

Kimoto (2009) Argo fields and residual patterns.

Figure 8 (A) and (B) display trend-maps of the combined (FESOM/Argo + residual) steric effect as estimated from the two inversions over the period 2004-2012 in the Indian Ocean. In the Bay of Bengal, both solutions indicate strong trends of about 10 mm/a along the east coast of India, coinciding with the southward transport of the seasonal freshwater plume that is associated with the annual monsoon (Vinayachandran et al., 2013). Additionally, both inversions detect strong positive trends of 5 to 10 mm/a in the central, southern and eastern parts of the Bay of Bengal. Small trends around 0 to 4 mm/a are found at the east-coast, as well as in a small band north-east of Sri Lanka. In the northern part of the bay at the coast of the Chittagong region (south-east Bangladesh) we identify trends close to zero.

In the remaining parts of the Indian Ocean, both inversion runs agree remarkably well (Fig. 8, (A) and (B)) with strong positive trends of about 10 mm/a in the Arabian Sea, especially at the coasts of Oman and Pakistan. Furthermore, strong positive trends (5-10 mm/a) are found in a band around the equator. Around the coasts of Madagascar and in a band at around $15°S$ of latitude and reaching east up to about $90°E$ of longitude, both inversion runs detect generally small trends around 0 mm/a and strong negative trends of -5 to -10 mm/a in some regions. In the southern Indian Ocean, strong positive trends can be found again. At longitudes east of $90°E$, at the coasts of Australia and Indonesia, both inversion solutions are consistent with very strong steric trends of more than 15 mm/a, which are significantly larger than the global mean steric trend.

However, there are some differences between INVERSION01 and INVERSION02. In the

Bay of Bengal, INVERSION02 finds slightly negative steric trends at the west- and south-coast of Myanmar, while INVERSION01 detects positive trends of more than 5 mm/a in the same regions. Furthermore, INVERSION01 finds trends close to zero at the coast of Bangladesh, while the model-based INVERSION02 detects strong positive trends, especially in the Sunderbans region. A similar reasoning can be applied to the south-east coast of India where INVERSION01 detects significantly smaller trends compared to INVERSION02.

At the west-coast of India, INVERSION02 indicates trends close to zero, while the Argo-based INVERSION01 detects strong positive trends up to 10 mm/a. Comparing the results close to the east-coast of Africa at about $5°S$, we find positive trends in INVERSION02 and trends close to zero in INVERSION01. At the coasts of Madagascar and in the band around $15°S$, INVERSION01 identifies four rather large regions with strong negative trends of up to -10 mm/a while INVERSION02 points at seven relatively smaller regions of negative trends in the same area.

Generally the largest differences in the steric trends occur at regions where only little Argo measurements are available (Church et al., 2010), such as coastal zones or regions with strong currents and eddies, e.g. at south tip of India or the eastern Bay of Bengal (e.g., Hacker et al., 1998). The FESOM model is independent from depth limitations or floater positions and provides values, and hence does the INVERSION02 result in more spatail details compared to INVERSION01.

HERE GOES FIG. 9

The trend maps in Fig. 9 display steric trends derived from our INVERSION01 (A) and INVERSION02 (B) each without the corresponding residual modes. In the Bay of Bengal, the steric trend derived from the FESOM-based modes already includes the strong positive trends along the east coast of India and the small trends east and north-east of Sri Lanka (Fig. 8, (B) and Fig. 9, (B)). At the same time, the residual modes of INVERSION02 add strong positive trends at the southern and eastern parts of the bay. For INVERSION01 (Fig. 8, (A) and Fig, 9, (A)), the steric trends associated with the upper 700 m of the ocean find positive trends of 0 to 5 mm/a in the southern two thirds of the Bay of Bengal, while small and even slightly negative trends are present in the northern third of the bay. Adding modes derived from altimetry residuals emphasizes the positive trends at the east coast of India and in the southern and eastern parts of the bay, while it diminishes trends east and north-east of Sri Lanka and adds positive trends, likely associated with the advection of the freshwater plume, to the north-west part of the bay up to the coast of the Sunderbans region in Bangladesh.

In the remaining part of the Indian Ocean, Fig. 8, (A) and (B), and Fig. 9, (A) and (B) all include the general large scale features that are present in the Indian Ocean, such as the positive trends around the equator, small to negative trends around Madagascar and in a band east of it at about $15°S$ latitude and strong positive trends of up to 15 mm/a at the coasts of Australia and Indonesia. These trends are emphasized when the residual dynamic modes are added, while in other regions, such as the Arabian Sea, the residual contributions might change the spatial trend patterns significantly, e.g. leading to strong positive trends in former small trend regions and vice versa. It is noteworthy that the steric results in INVERSION02 show only small to moderate trends in the southern Indian Ocean from $25°S$ to $30°S$ latitude (Fig. 9, (B)), which do not agree well with the trends based on INVERSION01 (Fig. 9, (A)). Yet, after adding the respective residual modes, both solutions show quite similar trends in this region (Fig. 8). This generally good agreement of both inversion solutions after reinstating the residual contributions stresses the importance of these extra fingerprints when reconstructing the total sea level in the Bay of Bengal and the Indian Ocean. Therefore, we believe they account for model weaknesses and locally important effects which are not well-captured by the Argo-based steric modes (e.g. they are either not captured by Argo fields due to insufficient sampling, or they are not captured in our inevitably limited number of EOF basefunctions), such as influences related to mass changes or from wind or IOD/ENSO events.

Additionally, Fig. 9 allows to compare the steric trends from the two global inversion runs to independent steric trend estimates based on the upper 700 m and same period of Argo data-sets from Ishii and Kimoto (2009) and INCOIS (Fig. 9, (C) and (D), respectively). When comparing (C) to (A), one should keep in mind that it is exactly this data set (but from 1992 to 2011) from which we had extracted the (normalized) leading modes of variability as base functions to be fitted to GRACE/altimetry. In other words, some similarity can be expected since the Ishii and Kimoto (2009) data and what INVERSION01 attributes to the upper 700 m (the fields shown in Fig. 9 ((A) and (C)) share the same mathematical subspace, but the time component is entirely independent.

In the Bay of Bengal, (A) and (C) agree well in the central part of the bay, while INVERSION01 attributes moderate positive trends to regions east and north-east of Sri Lanka, whereas small to slightly negative trends are found in the Ishii and Kimoto (2009) Argo dataset (C). These smaller trends in this region are also detected in the INCOIS data set (D) and in the trends based on the full-depth FESOM model (B); they also agree with small trends after addition of the residual contributions (Fig. 8). In the northern part of the bay, (A) and (C) both see small, slightly negative trends for the upper 700 m, while in (D) we find small up to moderate positive trends, especially at the coast of the Chittagong region, Bangladesh, in the north-eastern part of the bay; both inversion solutions find small trends after addition of the residual dynamic contributions (Fig. 8).

Comparisons in the remaining part of the Indian Ocean reveal regions of good agreement, such as positive trends in the eastern equatorial band and very strong positive trends at the coasts of Australia and Indonesia, between the inversions solutions (Fig. 9, (A) and (B)) and the the Argo-datasets (Fig. 9, (C) and (D)). However, there are regions, where the Argo derived trends do not agree well with the inversion solutions. In the western part of the equatorial band, as well as in the Arabian Sea, the trends based on Argo fields tend to detect significantly smaller trends (Fig. 9, (C) and (D)) compared to the INVERSION01 and INVERSION02. The INCOIS solution exhibits large positive tends of up to 12 mm/a at the east-coast of Madagascar while all other solutions attribute small or even moderate negative trends to the same region. At about $30°S$ latitude, the INCOIS solution indicates a band of strong negative trends of less than -15 mm/a from south-east of Madagascar up to $110°E$ longitude. The solutions INVERSION01, INVERSION02, and the Ishii and Kimoto (2009) Argo-dataset suggest strong positive trends of about 5 to 10 mm/a in this region. The gridded Argo-datasets include assumptions, background models and interpolation between the unevenly distributed Argo measurements, which lead to differences between the individual products. Here, these differences are in particular apparent in the western and southern parts of the Indian Ocean for the INCOIS data set.

In summary, in contrast to the Argo floats, which currently only measure the upper 2000 m of the ocean, our inversion based on GRACE and altimetry data should see the total integrated sea level change from the sea surface down to the seafloor. Therefore, in the inversion approach, a combination of Argo based steric fingerprints for the upper ocean (INVERION01) or steric fingerprints based on FESOM-model output (INVERSION02), combined with residual fingerprints that supposedly accounts for the deep ocean contribution as well as unmodeled effects, offers a new perspective on understanding steric sea level change.

HERE GOES FIG. 10

For the Bay of Bengal, Fig. 10 displays the temporal variation of steric anomalies from the GRACE/altimetry inversions INVERSION02 (model-based, blue) and INVERSION01 (Argo-based, orange) as well as from three independent datasets (black - Ishii and Kimoto (2009), green - upper 700 m from IPRC, and violet - upper 700 m from INCOIS). The figure reveals that our GRACE/altimetry inversion results (INVERSION01) for the upper ocean appear quite similar to those steric anomaly products that are based on Argo data , i.e. Ishii and Kimoto (2009), IPRC and INCOIS (correlations of 0.85) , while the results from INVERSION02 fit less well (correlations of 0.6-0.7). Before 2005, when the Argo network was very sparsely distributed, the Argo data-sets heavily relied on additional model data from climatological models and the results of the two inversions and from Ishii and Kimoto (2009) fit together quite well. From 2005 onward, the Argo network reached its targeted number of floats and the impact of these measurements on the gridded fields strengthens. Here, we find that the INVERSION02 steric anomalies agree in general with the other methods in the Bay of Bengal, but there are some larger discrepancies with respect to the other datasets. We hypothesize that the differences are related to the INVERSION02 fingerprints covering the total depth down to the seafloor, as well as to the FESOM model itself which is different from the background models used for deriving the Argo fields. At the same time, we believe this lends credibility to the GRACE/altimetry inversion method because the anomalies of INVERSION01 for the same depth range like the independent datasets agree well and anomalies derived from a non-Argo influenced, FESOM-model (INVERSION02) still show some level of agreement.

4.4. Mass contributions to sea level in the Bay of Bengal

Mass contributions to sea level in the Bay of Bengal, as inferred by global inversion of GRACE and altimetry data, can be investigated in two different ways. In what follows, we will first analyze sea level trend maps that originate from each of the major mass contributors (Greenland and Antarctica ice sheets, world glaciers and land hydrology) separately after partitioning in our inversion. Then, in a second experiment, we will compare basin averages for the Ganges and Brahmaputra basins (Fig. 12, A) from the inversion runs to basin averages based on conventional analysis of GRACE level-2 spherical harmonics.

HERE GOES FIG. 11

Figure 11 compiles four maps of mass-driven SLR in the Indian Ocean and in the Bay of Bengal (averaged trends of the different contributions in the Bay of Bengal have already been discussed in Section 4.1). We find the effect of Greenland mass loss to be relatively stable with about $0.7 - 0.8\,\mathrm{mm/a}$ in the larger Indian Ocean, while SLR originating from Antarctica mass loss is smaller in the Northern part and the Bay of Bengal (about $0.2 - 0.3\,\mathrm{mm/a}$) and larger (about $0.4 - 0.5\,\mathrm{mm/a}$) in the Southern Indian Ocean. Similar behavior can be found for SLR resulting from glacier melting, showing a gradual increase from about 0.4 mm/a in the northern part of the Indian Ocean, including the Bay of Bengal, to about 0.5 mm/a in the southern part. Mass-driven SLR resulting from land water storage changes show negative values of about $-0.3\,\mathrm{mm/a}$ in large parts of the Indian ocean, in line with global results that suggest that in the period since 2003 increasingly more water is stored on the continents (Llovel et al., 2010, Riva et al., 2010). Small positive trends of about 0.2 - 0.3 mm/a are found at the north-west coast of India in the Gujarat region, which agrees with positive mass trends and corresponding attraction of sea-water also found in GRACE data over this region (e.g. Cazenave and Chen, 2010).

In the northern Bay of Bengal, strong negative trends of -0.5 to -1.5 mm/a are identified along the estuaries of the GBM rivers and at the Sunderbans region. While effectively slowing sea level rise, these effects appear as a result of strong mass loss trends in the Ganges and Brahmaputra river basins, a part of which is likely related to widespread groundwater withdrawal in the Bengal region (Tiwari et al., 2009). This mass loss leads to a lowering of both the geoid and sea level along the coast of Bangladesh.

Next, we compute monthly basin averages (Sec. 3.2) from 2002 to 2014 using GFZ

RL05a GRACE fields. Following standard procedures, and in order to be consistent with the processing of GRACE data in the global inversion method, these fields have been augmented with C_{20} coefficients from satellite laser ranging (SLR) measurements (Cheng et al., 2013b) and with degree 1 coefficients derived from the inversion. This last modification effectively transforms the GRACE coefficients, which are provided in the center of mass (CM) reference frame, to the center of figure (CF) reference frame, which is required for the computation of equivalent water height change and used in our inversion. Additionally, a temporal mean field has been removed, the residual GRACE fields have been smoothed and decorrelated with the DDK3 filter (Kusche, 2007), and monthly basin averages have been computed for the Ganges and Brahmaputra basins (Fig. 12, A).

Jensen et al. (2013) report GRACE-derived mass trends of -22.6 Gt/a and -12.4 Gt/a between August 2002 and July 2009 for the Ganges and Brahmaputra basins, while here we find -19.5 Gt/a and -9.9 Gt/a for the same period and basins. These differences can be explained by the use of different releases of GRACE data and a slightly different rescaling approaches. Khan et al. (2012) investigated the lower Ganges basin and derived trends between April 2003 and April 2007 ranging from -24.24 mm/a to -29.46 mm/a for three $4^\circ \times 4^\circ$ tiles covering large parts of the Ganges basin. When focusing on the same time period, our trend estimate of -26.8 mm/a agrees well with the findings of Khan et al. (2012). Total water storage change from January 2003 to December 2007 within Bangladesh and India's West Bengal region has also been investigated by Shamsudduha et al. (2012). They estimated annual ranges of 49 cm and 58 cm using GRACE fields from the Groupe de Recherche en Géodesie Spatiale (GRGS) and from the Centre for Space Research of the University of Texas (CSR). Again, our result is in reasonable agreement with ranges of 44 cm and 40 cm for the same period in the Ganges and Brahmaputra basins, which both include parts of the Bengal basin used by Shamsudduha et al. (2012).

HERE GOES FIG. 12

In our global inverse method, we estimate the hydrology contribution to the total sea level based on mass-change patterns (and corresponding sea level fingerprints, consistent in a gravitationally-elastic sense) derived from a land hydrological model. Scaling these (normalized) a priori mass patterns with the time-variable amplitudes derived in the inversion from GRACE and altimetry, and averaging these subsequently over basin regions, enables us to derive continental total water storage changes comparable to the standard approach in the GRACE community. Here, we use 60 hydrological fingerprints derived from WGHM (Döll et al., 2003) EOFs, combined with fingerprints from glacial isostatic adjustment (GIA) modelling and the Himalaya glacier contribution, and compute basin averages as described in Section 3.2. These are then compared to basin averages derived from monthly GFZ RL05a GRACE solutions as described above.

Figure 12 (A) shows the the location and extent of the Ganges and Brahmaputra basins. A comparison of TWSC changes from the GRACE basin averaging approach and from our two inversion solutions in the Ganges basin (Fig. 12, B) reveals, as expected, that INVERSION01 and INVERSION02 arrive at nearly the same results. However, from 2002 to 2004, the inversion method seems to underestimate the TWSC change compared to the GRACE basin averaging solution in the Ganges basin (Fig. 12, B). Good agreement is then found between mid 2004 and 2012. A close look at the GRACE data reveales that less mass change originated from the Uttar Pradesh and Madhya Pradesh regions in northern India, where much groundwater has been withdrawn for agricultural purposes in the past (Fig. 2(a) in Döll et al., 2011). Apparently the inversion method is not able to account well for these small scale events, relying on globally defined fingerprints. Similar to the Ganges basin, the inversion seems to underestimate TWSC change between 2002 and 2005 in the Brahmaputra basin (Fig. 12, C). From 2005 onward the inversion and GRACE basin averaging results agree well, with best agreements in 2005, 2009 and 2013. The higher peak amplitudes in 2006, 2007, 2008, 2010 and 2011 may be associated with flooding events in the lower Brahmaputra basin, often connected to severe cyclones (e.g. Sidr in 2007). In addition, the skill of the WGHM model in representing floodings or the response to strong La Niña events, e.g. resulting 2010 in above-average rainfall and more water mass inside the basin, may be limited. Since we use WGHM for deriving the basis functions that are, in the inversion, fitted to GRACE data, hydrological modelling deficiencies might lead to poorer approximations in this basin.

In order to separate between short-term and long interannual variability, we applied a 12-month boxcar filter to the GRACE basin averaging and inversion averaged time series for the Ganges and Brahmaputra basins. Short-term signals directly derived from GRACE and from our inversions agree, for both basins, quite well with RMS of 28.0 Gt and 22.3 Gt , and correlations of 0.97 and 0.97 for the Ganges and Brahmaputra basin. A closer look at interannual changes (dashed lines in Fig. 12, B and C) reveals slightly positive apparent trends in both basins from 2002 to 2004, which shift to negative trends in 2004. Additionally, it is obvious that an underestimation of the mass change of the global inversion compared to the direct GRACE approach occurs in the long period part of the signal. The reason for this may be due to some general disagreement between TWSC changes derived from GRACE and WGHM from 2002 to 2003/04 (not shown here), especially in the Brahmaputra basin in 2003, which then propagate into the inversion results since the WGHM-derived fingerprints likely do not adequately explain the GRACE data. In the Brahmaputra basin, the inversion seems to be generally biased to a lower TWSC level compared to the direct GRACE results, pointing again to possible hydrological modelling problems in this region.

For the Ganges basin, over the entire GRACE time period (from 2002 to 2014) we find trends of -13.9 Gt/a and -7.8 Gt/a from GRACE basin averaging and from the inversion, respectively. For the Brahmaputra basin, we derive trends of -9.6 Gt/a and -6.4 Gt/a for the same time period. We identify and implement apparent trend changes in the Ganges and Brahmaputra basins in 2004 and 2005, respectively, which resulted in trends of -12.44 mm/a and -11.60 mm/a for 2004 to 2014 the Ganges basin and -9.37 mm/a and -9.78 mm/a for 2005 to 2014 in the Brahmaputra basin. Over this period, the inversion results show better agreement with the trends derived from GRACE only. Apparent trends from 2002 to 2004 and 2002 to 2005 for the Ganges and Brahmaputra basins show good agreement, but are not shown here, since they are considered less meaningful.

Comparisons to the estimates labelled as “InvEOF” in Jensen et al. (2013) are summarized in Tab. 3; they reveal good agreement with the direct GRACE basin averaging, while the trend based on our inversion differs, likely as a result of the underestimation during 2002 to 2004. For the Brahmaputra basin, the trend (August, 2002 to July, 2009) from Jensen et al. (2013) even shows a different sign compared to trends derived directly from GRACE and from the inversion.

HERE GOES TAB. 3

4.5. Future changes

Finally, we attempt to predict the future evolution of absolute sea level in the Bay of Bengal, up to the year 2050. To this end, we combine present-day regional trends as inferred from altimetry and GRACE in previous sections (Tab. 2) with likely changes of sea level rates for the steric contribution as well as for the mass effects of Greenland, Antarctica, land hydrology and the world's glaciers, all evaluated for the Bay of Bengal.

HERE GOES TAB. 4

For the mass-related accelerations, we use our regional estimates over 2002-2014 (Tab. 4) estimated consistently with trends that were discussed before. For Bay of Bengal SLR contributions from land hydrology, Greenland and Antarctica we find accelerations of $0.03\,\mathrm{mm/a^2}$, $0.03\,\mathrm{mm/a^2}$ and $0.01\,\mathrm{mm/a^2}$, respectively, which is of the same order of magnitude compared to accelerations derived for global mean SLR. However, for the glacier contribution we find the acceleration in the considered time period to be not significantly different from zero, in both the Bay and in the global mean; therefore we will only consider the glacier mass loss trend. Combining all mass contributions, we find a trend of $1.17\,\mathrm{mm/a}$ and a corresponding acceleration of $0.07\,\mathrm{mm/a^2}$.

We notice that our accelerations are somewhat smaller compared to those estimated by Rignot et al. (2011) based on the 1992-2010 time frame, very likely due to the different data period: for Greenland and Antarctica they find accelerations of $0.057\,\mathrm{mm/a^2}$ and $0.038\,\mathrm{mm/a^2}$. For the glacier contribution Rignot et al. (2011) provide an estimate of $0.031\,\mathrm{mm/a^2}$; the land hydrology contribution is not considered in their study.

For the future acceleration of the thermo- and halosteric contributions to SLR, we turn to model runs provided in the fifth phase of the Coupled Model Intercomparison Project (CMIP5) on a global scale (`http://esgf-data.dkrz.de/esgf-web-fe/`). Due to computational reasons we limit ourselves to using only the outputs from the Max Planck Institute for Meteorology (MPI-M) model runs, which, in the global mean, appear fairly in the center of the CMIP5 multimodel ensembles. Utilizing methods outlined in Section 3.1, we compute gridded monthly steric sea level heights from 2006 to 2050 for each of the three Representative Concentration Pathways (RCP) scenarios RCP2.6, RCP4.5 and RCP8.5. Indeed we find the steric sea level in the Bay of Bengal (Tab. 4) to accelerate faster compared to the global average under all three scenarios.

The last column in Tab. 4 reports the expected sea level rise in the Bay of Bengal in 2050 relative to 2005 for the individual mass components and their combined total, as well as for the steric component under the assumption of different RCP scenarios. Adding steric and mass-related projections, we suggest that the absolute sea level in the Bay of Bengal may rise up to about 40 cm under the RCP8.5 scenario, about 37 cm under RCP4.5 and about 27 cm under the RCP2.6 scenario. This is less than the upper-end scenario of 50 cm sea level rise by 2050 suggested in World Bank (2000) while it is well in range with the

SLR of 32 cm in 2050 adopted by the National Adaption Programme of Action by the Ministry of Environment and Forest of the Government in Bangladesh (MOEF, 2005). Compared to global mean IPCC AR5 estimates (Church et al., 2013), which report SLR increase ranging from 0.24 cm to 0.30 cm for the time period 2046-2065 relative to 1986-2005, our estimates derived here for the Bay of Bengal appear somewhat larger and at the upper end of the reported confidence intervals for each of the RCP scenarios in the AR5.

Of course, it is unclear as to what extent the current mass loss trends and accelerations reflect long-term evolution or decadal variability, and our estimates should be seen as upper limits given the present data. Furthermore, the mentioned numbers refer to absolute SLR. To this, vertical land motion would add a largely unknown contribution. When we consider the mean GBM delta subsidence rate found by Brown and Nicholls (2015), relative sea level would rise additionally by approx 13 cm along the Bay of Bengal.

5. Conclusions

We have assessed mass and steric contributions to sea level variability in the Bay of Bengal, using Jason 1/2 radar altimetry and GRACE data in an inverse approach developed in Rietbroek et al. (2012). We find total sea level rates more than twice above global average, with the steric contribution dominating over mass-driven effects. In total, our inversion explains more than 90% of the observed SLR; however some uncertainty remains in attributing certain residual modes found in altimetric height change to steric sea level change or to other possible sources.

The steric contribution that we find compares quite well to independent, Argo-based steric heights that, however, do not consider the full ocean depth, when we base the solution space of the inversion on Argo-derived patterns. It compares less well when our solution space is based on ocean modelling. We therefore suggest that a sizeable part of SLR should be ascribed to sources other than contained in Argo data, such as deep ocean warming, internal mass redistribution, or wind effects.

The mass contribution to SLR in the Bay of Bengal (1.17 mm/a to 1.29 mm/a) appears fairly on par with global averages. Changes in (global) land hydrological storage accounts for a negative contribution (i.e. sea level fall) of -0.23 mm/a to -0.31 mm/a. We find that the total water storage change in the Ganges and Brahmaputra river basins reconstructed from the inversion compares well to GRACE-only data; in fact our inverse estimates point at somewhat lower values compared to the direct GRACE basin-averaging approach.

The main conclusion from this study is that regional estimates obtained in a global inverse framework, consistent with self-gravitation, elastic loading and reference frame theory, and the rotational feedback of the Earth, can be successfully validated with regional and in-situ data sets. For the Bay of Bengal, this approach leads to a partitioning of sea level that fits well to independent results and provides new insights into the processes driving SLR.

On the basis of this partitioning, we assess future (absolute) sea level rise in the Bay of Bengal and find likely rise for the 2050 framework somewhat larger compared to global averages from IPCC AR5, but slightly less compared to some other regional estimates.

A. Inverse Method for Partitioning Altimetric Sea Level Change

A.1. Fingerprints

In the inverse method (Rietbroek et al., 2012), individual mass contributions to sea level change are parameterized through predefined, normalized, spatially invariant patterns or fingerprints. For these patterns, time-varying scalings are then estimated by fitting to GRACE spherical harmonics and Jason 1/2 binned along-track altimetry in a least squares approach, together with steric patterns.

In our current setup, mass contributions are discretized by 119 global fingerprints, of which 27 and 16 relate to basins in Antarctica and Greenland, 16 to major glacier clusters (from WGI/GLIMS database, Raup et al., 2007), and 60 to land water storage change. Each individual fingerprint represent a passive ocean response derived through the Sea Level Equation (see eq. (A.1), Farrell and Clark, 1976). This equation relates load mass change δh at location λ', θ' to changes in sea level $\delta s(\lambda, \theta, t)$

$$\begin{aligned}\delta s(\lambda,\theta,t) =&O(\lambda,\theta)\int_\Omega G^L_{N-U}(\delta s(\lambda',\theta',t)+dh(\lambda',\theta',t))d\omega \\ &+\int_\Omega G^T_{N-U}\delta\Lambda(\delta s,\delta h)d\omega+\frac{\Delta V}{g}.\end{aligned} \tag{A.1}$$

Eq. (A.1) accounts for self-gravitation as well as the effect of the changing rotational potential $\delta\Lambda$ (rotational feedback): The Green's functions G^L_{N-U} and G^T_{N-U} model the elastic response of the Earth to loading (L) and potential forcing (T), in terms of geoid change N with respect to the elastically uplifting/subsiding ocean bottom and land surface U. In Eq. (A.1), $O(\lambda,\theta)$ represents the ocean function. In order to conserve mass, $\frac{\Delta V}{g}$ allows for a uniform shift with respect to the geoid. The numerical approach that we employ to solve the Sea Level Equation in the spectral domain is described in detail in

Rietbroek et al. (2012), Jensen et al. (2013), and Rietbroek (2014).

In order to solve for steric changes, we prescribe 100 (200) empirical orthogonal functions (EOFs) in the inversion INVERSION01 (INVERSION02). EOFs are based on steric sea level heights derived from integrating the temperature and salinity changes over depths from 0-700 m, from 1° gridded Argo-data (v6.31, Ishii and Kimoto, 2009) and 0 m down to sea floor from the FESOM model (Timmermann at al., 2009), interpolated to a $0.5° \times 0.5°$ grid.

Instead on relying on a single a priori model of glacial isostatic adjustment (GIA), we fit five individual GIA fingerprints to the data, associated with the major former glacial regions Laurentide, Antarctica, Greenland, Fernoscandia, and other glacial masses. These patterns were computed by V. Klemann following (Klemann and Martinec, 2009) for separate (ICE5G) mass load histories, VM2-2 rheology, and kindly provided to us. GIA is thus estimated as a linear trend over the total time period, for each of the five regions.

Furthermore, after an initial inversion, we derive and apply an additional set of (here: 100) leading EOFs from (200 km-) Gaussian smoothed altimetry residuals. This allows, to some extent, to separate unmodeled but spatially coherent effects, e.g. residual ocean dynamics, from 'noise'. In the following step, these residual fingerprints are then introduced into the estimation along with all other patterns.

A.2. Least Squares Fit

Monthly scaling factors are derived through least squares estimation. We combine GRACE data and altimetry on a normal equation level, taking into account all correlations that result from orbital patterns. Therefore, GRACE normal equations which originally refer to spherical harmonics have to be related to fingerprints. The GRACE monthly spherical harmonics δC_{nm} relate to mass fingerprints through

$$\delta C_{nm}(t) = \mathbf{D} \begin{bmatrix} \mathbf{x}_{ice}(t) \\ \mathbf{x}_{glac}(t) \\ \mathbf{x}_{hydr}(t) \\ (t - t_0)\mathbf{x}_{gia} \end{bmatrix} + \epsilon, \tag{A.2}$$

where $\mathbf{D}$ contains the harmonic coefficients of the fingerprints. $\mathbf{x}_{ice}(t)$, $\mathbf{x}_{glac}(t)$ and $\mathbf{x}_{hydr}(t)$ represent the monthly scalings, and $\mathbf{x}_{gia}$ includes trends for the GIA regions over the inversion time period, referring to mid-epoch t_0. For the actual estimation, we utilize the full (unsolved and unfiltered) normal equation systems complete up to degree/order 150 provided by GFZ Potsdam (RL 05a), transformed using $\mathbf{D}$. Steric changes do not have to be considered in Eq. (A.2) since GRACE is insensitive to volumetric changes.

Jason-1/2 sea level anomalies (SLA) are derived from the Radar Altimetry Database System (RADS, Scharroo et al., 2013), with all standard atmospheric and geophysical corrections applied. However, atmospheric pressure loading has been removed from altimetry consistent with GRACE processing, where so-called GAC background model output is applied. Then, along-track observations are averaged into bins of about 6 km length. SLA $\delta h_{SLA}(t)$ relates to the individual fingerprints through

$$\begin{aligned} \delta h_{SLA}(t) = & \mathbf{YB} \begin{bmatrix} \mathbf{x}_{ice}(t) \\ \mathbf{x}_{glac}(t) \\ \mathbf{x}_{hydr}(t) \\ (t - t0)\mathbf{x}_{gia} \end{bmatrix} + \mathbf{KC} \begin{bmatrix} \mathbf{x}_{steric}(t) \\ \mathbf{x}_{unexpl}(t) \end{bmatrix} + \\ & \mathbf{P} \begin{bmatrix} x_{satbias} \end{bmatrix} + \epsilon. \end{aligned} \tag{A.3}$$

Here, mass-related scalings are as above, and $\mathbf{B}$ contains the corresponding fingerprints expressed in geocentric sea level. Matrix $\mathbf{Y}$ maps the spherical harmonic coefficients in $\mathbf{B}$ to the bin positions. Gridded steric and residual fingerprints are contained in matrix $\mathbf{C}$, and are mapped to bin positions by bi-linear interpolation (matrix $\mathbf{K}$), which then relates the steric ($\mathbf{x}_{steric}$) and residual ($\mathbf{x}_{unexpl}$) monthly scalings to the binned sea level anomalies. In Eq. (A.3) we also include altimeter-specific offsets $x_{satbias}$, and are projected onto the radial direction by $\mathbf{P}$.

Our weighting scheme utilizes the full GRACE error covariance (as repesented in the normal equations, i.e. all correlations between harmonic coefficients that result from time-varying orbit repeat regimes are accounted for) and a diagonal covariance matrix that weights the bin-wise SLA errors. GRACE and altimetry normal equations are subsequently combined, but some constraints have to be added due to correlations between adjacent smaller basins in Antarctica and Greenland, and also to aid the separation of GIA and present-day mass loss in Antarctica. Yet, these regularizations were designed to constrain differences (Rietbroek, 2014) and to keep the overall mass constraint of adjacent basins unconstrained, thus this procedure has little effect on estimated sea level change. Finally, all errors are propagated to the estimated scales and regional sea level contributions.

6. References

Alam, M. (1996): Subsidence of the Ganges-Brahmaputra delta of Bangladesh and associated drainage, sedimentation and salinity problems, in Sea level rise and coastal subsidence, Eds. Milliman, J.D. and B. U. Haq, Kluwer

Brown, S. and Nicholls, R.J. (2015): Subsidence and development in mega deltas: The case of the Ganges-Brahmaputra-Meghna. Science of the Total Environment, accepted

Cazenave, A. and Chen, J. (2010): Time-variable gravity from space and present-day mass redistribution in the Earth system. Earth and Planetary Science Letters, 298:263-274

Chen, J., Wilson, C., and Tapley, B.D. (2013): Contribution of ice sheet and mountain glacier melt to recent sea level rise. Nature Geoscience, 6:549-552

Cheng, X., Xie, S.-P., McCreary, J., Qi, Y., and Du, Y. (2013a): Intraseasonal variability of sea surface height in the Bay of Bengal. J. Geophys. Res. (Oceans) 118:816-830

Cheng, M, Tapley, B.D., and Ries, J. (2013b): Deceleration in the Earth's oblateness. J. Geophys. Res. (Solid Earth), 118(2):740-747

Church, J.A., Roemmich, D., Domingues, C.M., Willis, J.K., White, N.J., Gilson, J.E., Stammer, D., Köhl, A., Chambers, D.P., Landerer, F.W., Marotzke, J., Gregory J.M., Suzuki T., Cazenave, A., and Le Traon P.-Y. (2010): Ocean temperature and salinity contributions to global and regional sea-level change, in Understanding sea-level rise and variability, Eds. Church, J.A., Woodworth, P.L., Aarup, T., Wilson, W.S., Wiley-Blackwell

Church, J.A., Clark, P., Cazenave, A., Gregory, J.M., Jevrejeva, S., Levermann, A., Merrifield, M.A., Milne, G., Nerem, R.S., Nunn, P.D., Payne, A.J., Pfeffer, W.T., Stammer, D., and Unnikrishnan, A.S. (2013): Sea level change. In: Climate Change 2013: The Physical Science Basis. Contribution of Working Group I to the Fifth Assessment Report of the Intergovernmental Panel on Climate Change [Stocker, T.F., Qin, D., Plattner, G.-K., Tignor, M., Allen, S.K., Boschung, J., Nauels, A., Xia, Y., Bex, V., and Midgley, P.M. (eds.)]. Cambridge University Press, Cambridge, United Kingdom and New York, NY, USA, 11371216

Dee, D. P., Uppala, S. M., Simmons, A. J., Berrisford, P., Poli, P., Kobayashi, S., Andrae, U., Balmaseda, M. A., Balsamo, G., Bauer, P., Bechtold, P., Beljaars, A. C. M., van de Berg, L., Bidlot, J., Bormann, N., Delsol, C., Dragani, R., Fuentes, M., Geer, A. J., Haimberger, L., Healy, S. B., Hersbach, H., Holm, E. V., Isaksen, L., Kallberg, P., Köhler, M., Matricardi, M., McNally, A. P., Monge-Sanz, B. M., Morcrette, J.-J., Park, B.-K., Peubey, C., de Rosnay, P., Tavolato, C., Thpaut, J.-N., and Vitart, F. (2011): The ERA-Interim reanalysis: configuration and performance of the data assimilation system. Quarterly Journal of the Royal Meteorological Society 137, doi:10.1002/qj.828

Dieng, H., Palanisamy, H., Cazenave, A., Meyssignac, B., and von Schuckmann, K. (2015): The sea level budget since 2003: inference on the deep ocean heat content. Surveys in Geophysics, doi:10.1007/s10712-015-9314-6

Döll, P., Kaspar, F., and Lehner, B. (2003): A global hydrological model for deriving water availability indicators: model tuning and validation. Journal of Hydrology, 270(1-2):105-134.

Döll, P., Hoffmann-Dobrev, H., Portmann, F.T., Siebert, S., Eicker, A., Rodell, M., Strassberg, G., and Scanlon, B.R. (2011). Impact of water withdrawals from groundwater and surface water on continental water storage variations. Journal of Geodynamics, 59-60:143-156

Durand, F., Papa, F., Rahman, A., and Bala, S.K. (2011): Impact of Ganges-Brahmaputra interannual discharge variations on Bay of Bengal salinity and temperature during 1992-1999 period. J. Earth Syst. Sci. 120(5):859-872

Ericson, J., Vörösmarty, C., Dingman, S., Ward, L., and Meybeck, M. (2006): Effective sea-level rise and deltas: Causes of change and human dimension implications. Global and Planetary Change, 50:63-82

Farrell, W.E. and Clark, J.A. (1976): On postglacial sea level, Geophysical Journal of the Royal Astronomical Society, 46(3):647-667

Fenoglio-Marc, L., Rietbroek, R., Grayek, S., Becker, M., Kusche, J., and Stanev, E. (2012): Water mass variation in the Mediterranean and Black Seas, Journal of Geodynamics, 59-60:168-182

Hacker, P., Firing, E., Hummon, J., Gordon, A.L., and Kindle, J.C. (1998): Bay of Bengal currents during the northeast monsoon. Geophysical Research Letters, 25(15):2769-2772

Hacker, P., Maximenko, N., Potemra, J., Lebedev, K., DeCarlo, S., and Shen, Y. (2010): Argo and synthesis products developed and served at the Asia-Pacific Data Research Center, in: Proceedings of OceanObs'09: Sustained ocean observations and information for society (Annex), [Hall, J., Harrison, D.E., and Stammer, D. (eds.)], ESA Publication WPP-306

Han, W. and Webster, P. (2002): Forcing mechanisms of sea level interannual variability in the Bay of Bengal, Journal of Physical Oceanography, 32:216-239

Holgate, S.J., Matthews, A., Woodworth, P. L., Rickards, L. J., Tarnisiea, M. E., Bradshaw E., Foden, P. R., Gordon, K. M., Jevrejeva, S., and Pugh, J. (2013): New Data Systems and Products at the Permanent Service for Mean Sea Level. J. Coastal Res. 29 (3), pp. 493-504. doi:10.2112/JCOASTRES-D-12-00175.1.

International Hydrographic Organization (1953): Limits of oceans and seas, Special Publication No 23

Ishii, M. and Kimoto, M. (2009): Reevaluation of historical ocean heat content variations with time-varying XBT and MBT depth bias corrections. J. Oceanogr. 65(3):287-299

Islam, M., Begum, S., Yamaguchi, Y., and Ogawa, K. (1999): The Ganges and Brahmaputra rivers in Bangladesh: basin denudation and sedimentation, Hydrological Processes, 13:2907-2923

Jensen, L., Rietbroek ,R., and Kusche, J. (2013): Land water contribution to sea level from GRACE and Jason-1 measurements. J. Geophys. Res. (Oceans) 118(1):212226

Johnson, G. and Chambers, D. (2013): Ocean bottom pressure seasonal cycles and decadal trends from GRACE release-05: Ocean circulation implications. J. Geophys. Res. (Oceans) 118:4228-4240

Karim M.F. and Mimura, N. (2008): Impacts of climate change and sea-level rise on cyclonic storm surge floods in Bangladesh. Global Environmental Change 18:490-500

Khan, H.H., Khan, A., Ahmed, S., Gennero, M.C., Minh, K.D., and Cazenave, A. (2012): Terrestrial water dynamics in the lower Ganges - estimates from ENVISAT and GRACE. Arab J. Geosci, doi:10.1008/s12517-012-0629-z

Klees, R., Zapreeva, E., Winsemius, H., and Savenije, H. (2007): The bias in GRACE estimates of continental water storage variations. Hydrol. Earth Syst. Sci. 11:1227-1241

Klemann, V. and Martinec, Z. (2009): Contribution of glacial-isostatic adjustment to the geocenter motion. Tectonophysics, 511(3-4): 99-108

Kusche, J. (2007): Approximate decorrelation and non-isotropic smoothing of time-variable GRACE-type gravity field models. Journal of Geodesy, 81(11):733-749

Lee, S.-L., Park, W., Baringer, M., Gordon, A., Huber, B., and Liu, Y. (2015): Pacific origin of the abrupt increase in Indian Ocean heat content during the warming hiatus, Nature Geoscience, doi:10.1038/NGEO2438

Llovel, W., Becker, M., Cazenave, A., Cretaux, J., and Ramillien, G. (2010): Global land water storage change from GRACE over 2002-2009; Inference on sea level. C.R. Geosci. 342(3):179-188

Llovel, W., Meyssignac, B., and Cazenave, A. (2011): Steric sea level variations over 2004-2010 as a function of region and depth: Inference on the mass component variability in the North Atlantic Ocean. Geophys. Res. Lett. 38, L15608

McDougall, T.J. and Barker, P.M. (2011): Getting started with TEOS-10 and the Gibbs Seawater (GSW) Oceanographic Toolbox, 28 pp., SCOR/IAPSO WG 127

MOEF (2005): National adaption programme of action. Final Report, Ministry of Environment and Forest, Government of Bangladesh.

Mohal, N., Khan, Z.H., and Rahman, N. (2006) Impact of sea level rise on coastal rivers of Bangladesh, Institute of Water Modelling, Dhaka

Papa, F., Durand, F., Rossow, W.B., Rahman, A., and Bala, S.K. (2010): Satellite altimeter-derived monthly discharge of the Ganga-Brahmaputra River and its seasonal to interannual variations from 1993-2008. Journal of Geophysical Research, 115, C12013

Permanent Service for Mean Sea Level (PSMSL), (2015): Tide gauge data. Retrieved 18 Aug 2015 from http://www.psmsl.org/data/obtaining/

Purkey, S. and Johnson, G. (2010): Warming of global abyssal and deep southern ocean waters between the 1990s and 2000s: Contribution to global heat and sea level rise budgets. Journal of Climate 23:6336-6351

Raup, B., Racoviteanu, A. Khalsa, S., Helm, C.R.A., and Arnaud, Y. (2007): The GLIMS geospatial glacier database: A new tool for studying glacier change. Global and Planetary Change 56, 101.

Rietbroek, R., Brunnabend, S.-E., Kusche, J., and Schröter, J. (2012): Resolving sea level contributions by identifying fingerprints in time-variable gravity and altimetry. Journal of Geodynamics, 59-60:72-81

Rietbroek, R. (2014): Retrieval of sea level and surface loading variations from geodetic observations and model sumulations: an integrated approach. PhD thesis, University of Bonn

Rignot, E., Velicogna, I., van den Broeke, M.R., Monaghan, A., and Lenaerts, J. (2011): Acceleration of the contribution of the Greenland and Antarctic ice sheets to sea level rise. Geophysical Research Letters, 38, L05503

Riva, R., Bamber, J., Lavalee, D., and Wouters, B. (2010): Sea level fingerprint of continental water and ice mass change from GRACE. Geophys. Res. Lett. 37(19), doi:10.1029/2010GL044770

Scharroo, R., Leuliette, E.W., Lillibridge, J.L., Byrne, D., Naeije, M.C., and Mitchum, G.T. (2013). RADS: Consistent multi-mission products, in Proc. of the Symposium on 20 Years of Progress in Radar Altimetry, Venice, 20-28 September 2012, Eur. Space Agency Spec. Publ., ESA SP-710, p. 4 pp.

Singh, O.P (2006): ENSO and monsoon induced sea level changes and their impacts along the Indian coastline. Ind. Journal of Marine Sciences 35(2):87-92

Shamsudduha, M., Taylor, R.G., and Longuevergne, L. (2012): Monitoring groundwater storage changes in the highly seasonal humid tropics: Validation of GRACE measurements in the Bengal Basin. Water Resources Research 48, W02508

Slangen, A., Katsman, C., van de Wal, R., Vermeersen, L., and Riva, R. (2012): Towards regional projections of twenty-first century sea-level change based on IPCC SRES scenarios, Clim. Dyn. 38:1191-1209

Sreenivas, P., Gnasaseelan, C., and Prasad, K. (2012): Influence of El Nino and Indian Ocean Dipole on sea level variability in the Bay of Bengal, Global and Planetary Change 80-81:215-225

Steckler, M.S., Nooner, S.L., Akhter, S.H., Chowdhury, S.K., Bettadpur, S., Seeber, L., and Kogan, M.G. (2010) Modelling Earth deformation from monsoonal flooding in Bangladesh using hydrographic, GPS, and Gravity Recovery and Climate Experiment (GRACE) data, Journal of Geophysical Research (Solid Earth), 115:2156-2202

Syvitski, J., Kettner, A., Overeem, I., Hutton, E., Hannon, M., Brakenridge, G., Day, J., Vörösmarty, C., Saito, Y., Giosan, L., and Nicholls, R. (2009): Sinking deltas due to human activities, Nature Geoscience, 2:681-686

Thomas, M. (2002): Ocean induced variations in Earth rotation – Results from a simulataneous model for circulation and tides, PhD thesis, University of Hamburg, Germany

Tiwari, V.M., Wahr, J., and Swenson, S. (2009): Dwindling groundwater resources in northern India, from satellite gravity observations, Geophys. Res. Lett. 36, L18401, doi:10.1029/2009GL039401

Timmermann, R., Danilov, S., Schröter, J., Böning, C., Sidorenko, D., and Rollenhagen, K. (2009), Ocean circulation and sea ice distribution in a finite element global sea ice-ocean model, Ocean Modelling, 27(3-4):114-129.

Udaya Bhaskar, T.V.S., Ravichandram, M., and Devender, R. (2007): An operational Objective Analysis system at INCOIS for generation of Argo value added products. Technical Report No. INCOIS/MOG-TR-2/07, Indian National Center for Ocean Information Services

Vinayachandran, P.N., Shankar, D., Vernekar, S., Sandeep, K.K., Amol, P., Neema, C.P., and Chatterjee, A. (2013), A summer monsoon pump to keep the Bay of Bengal salty, Geophys. Research Letters, 40:1777-1782

Vinogradova, N., Ponte, R., Tamisea, M., Davis, J., and Hill, E. (2010): Effects of self-attraction and loading on annual variations of ocean bottom pressure. Journal of Geophysical Research (Oceans) 115:C06025, doi:10.1029/2009JC005783

Wahr, J., Molenaar, M., and Bryan, F. (1998): Time variability of the Earth's gravity field: Hydrological and oceanic effects and their possible detection using GRACE. Journal of Geophysical Research 103:30205-30230

World Bank (2000) Bangladesh, climate change and sustainable Development, report No. 21104-BD

World Bank (2011) The cost of adapting to extreme weather events in a changing climate, Bangladesh Development Series, paper no. 28

Acknowledgments.

We acknowledge financial support by DFG (Grants KU 1207/9-2 and 19-1) under the priority program SPP1257 and under the Belmont Forum CRA on Coastal Vulnerability. Thanks go also to all team members of the Band-Aid consortium (www.band-aid.org). Argo data were collected and made freely available by the International Argo Program and the national programs that contribute to it (http://www.argo.ucsd.edu, http://argo.jcommops.org). The Argo Program is part of the Global Ocean Observing System. In particular, we thank IPRC and INCOIS for providing value-added data derived from Argo. We would further like to thank the German Space Operations Center (GSOC) of the German Aerospace Center (DLR) for providing continuously and nearly 100% of the raw telemetry data of the twin GRACE satellites. Moreover, we are grateful to Ch. Dahle and F. Flechtner (GFZ Potsdam) for providing the GRACE RL05a normal equations that allow us to account for GRACE error characteristics and correlation patterns in our inverse method. We further acknowledge the World Climate Research Programme's Working Group on Coupled Modelling, responsible for CMIP, and we thank the climate modelling group MPI-M for producing and making available their model output. For CMIP the U.S. Department of Energy's Program for Climate Model Diagnosis and Intercomparison provides coordinating support and led development of software infrastructure in partnership with the Global Organization for Earth System Science Portals.

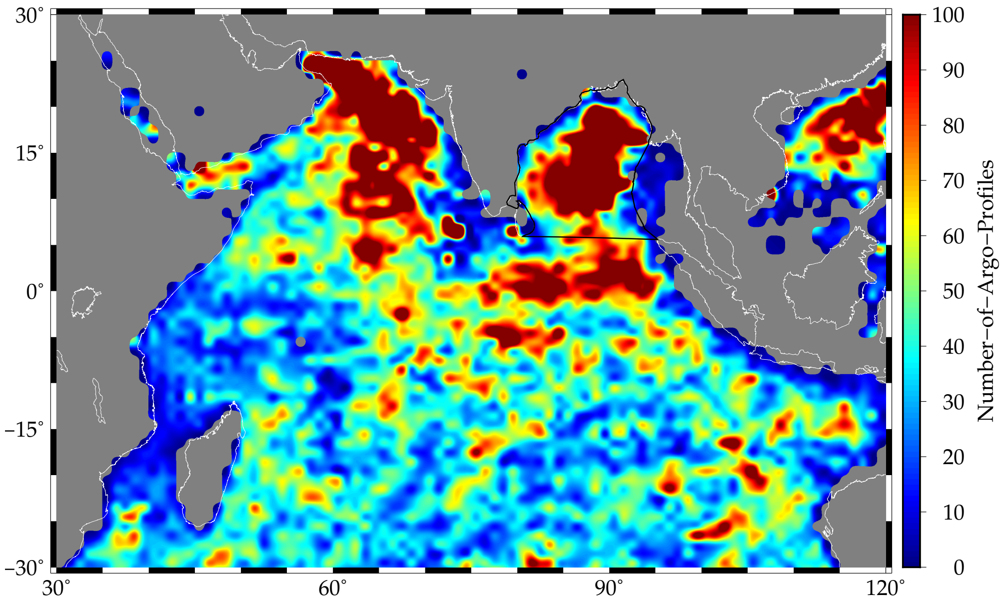

Figure 1. Argo profile density between 2002 and 2014. The total number of measured 10-day Argo profiles in each $1^\circ \times 1^\circ$ grid cell, capped at 100 profiles, is given.

Table 1. Absolute sea level trends, 2002 - 2014, global and in the Bay of Bengal. 1-Sigmas are formal; i. e. derived by propagating of instrumental errors. INVERSION01 used Argo-derived steric fingerprints, whereas INVERSION02 is based on model-derived fingerprints

	Global $[\frac{mm}{a}]$	Bay of Bengal $[\frac{mm}{a}]$
Altimetry	2.52 ± 0.07	6.1 ± 0.1
INVERSION01	2.40 ± 0.07	5.61 ± 0.65
INVERSION02	2.61 ± 0.08	5.85 ± 0.72

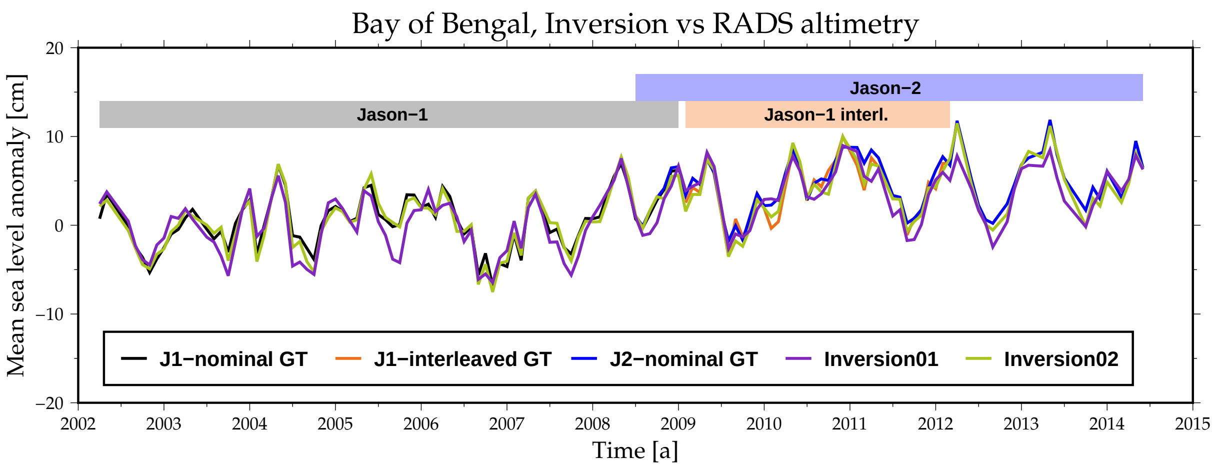

Figure 2. Altimetric sea level anomalies and total sea level reconstructed from inversion runs (Argo-Inv = INVERSION01, based on Argo-derived steric patterns, FESOM-Inv = INVERSION02, based on model-derived pattern) in the Bay of Bengal, 2002 - 2014.

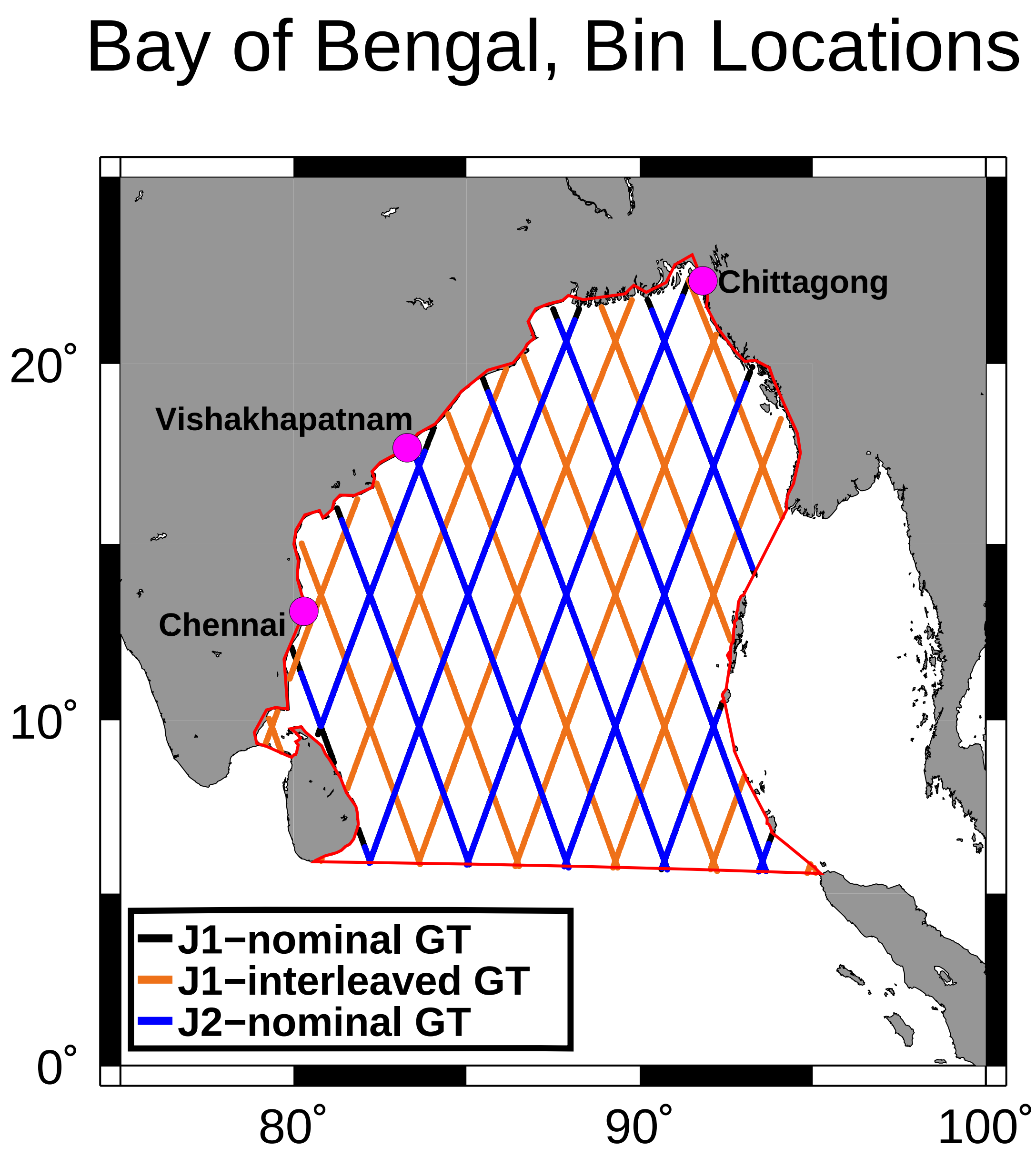

Figure 3. RADS bin locations in the Bay of Bengal

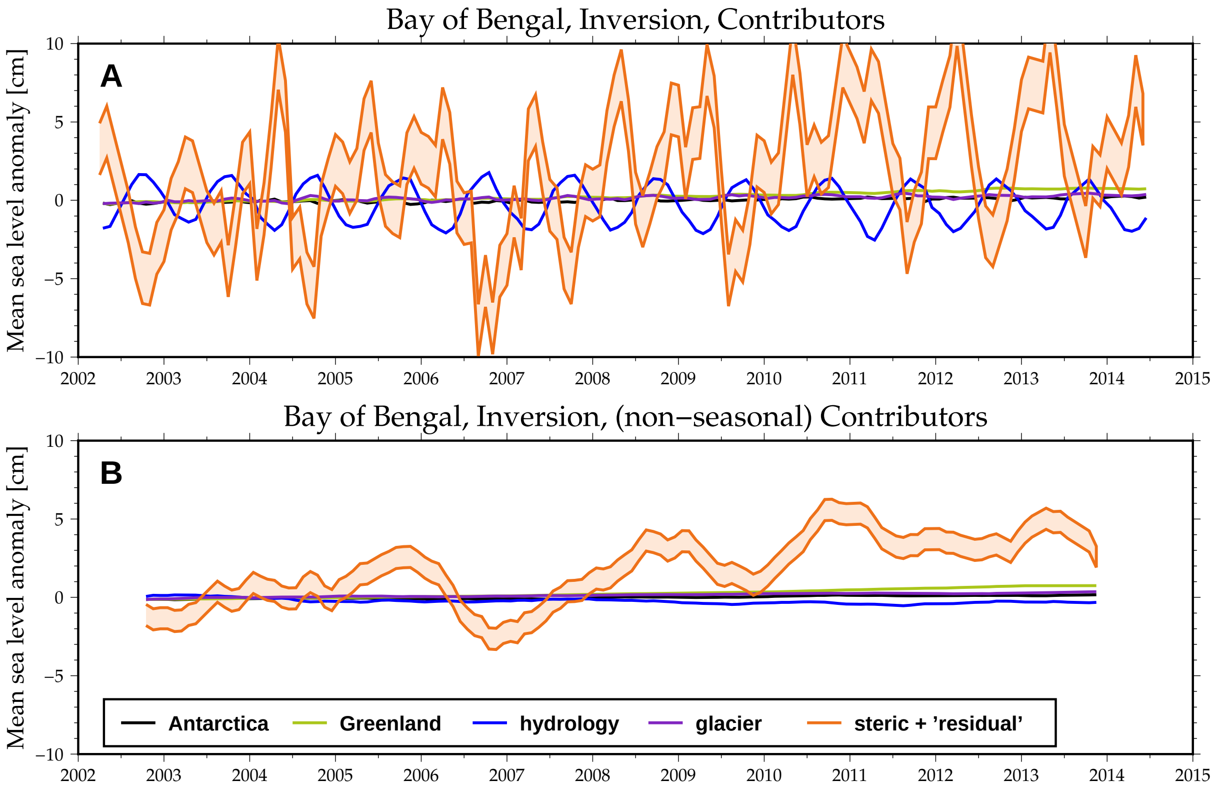

Figure 4. Top: Temporal variation of the contributions to the absolute sea level from Antarctica, Greenland, hydrology, glaciers and steric changes, 2002 - 2014, in the Bay of Bengal. Bottom: Annual harmonic fit removed and filtered with a 12 month boxcar filter. For the steric INVERSION02 component, half of the RMS difference between INVERSION01 and INVERSION02 steric components is shown as error. The differences of the mass contributions are negligible.

Table 2. Absolute sea level (ASL) trends, 2002 - 2014, of the different contributions in the Bay of Bengal (BoB). 1-sigmas are derived by propagation of instrumental errors.

	ASL INVERSION01 $[\frac{mm}{a}]$	**ASL INVERSION02** $[\frac{mm}{a}]$
Antarctica	0.30 ± 0.02	0.28 ± 0.02
Greenland	0.85 ± 0.01	0.84 ± 0.01
Hydrology	-0.23 ± 0.05	-0.31 ± 0.05
Glaciers	0.37 ± 0.02	0.36 ± 0.02
Steric	2.22 ± 0.65	3.08 ± 0.70
residual dynamics	2.07 ± 0.49	1.29 ± 0.49
steric + residual	4.29 ± 0.66	4.61 ± 0.77
total	5.52 ± 0.65	5.44 ± 0.74
total_binned	5.61 ± 0.65	5.86 ± 0.72

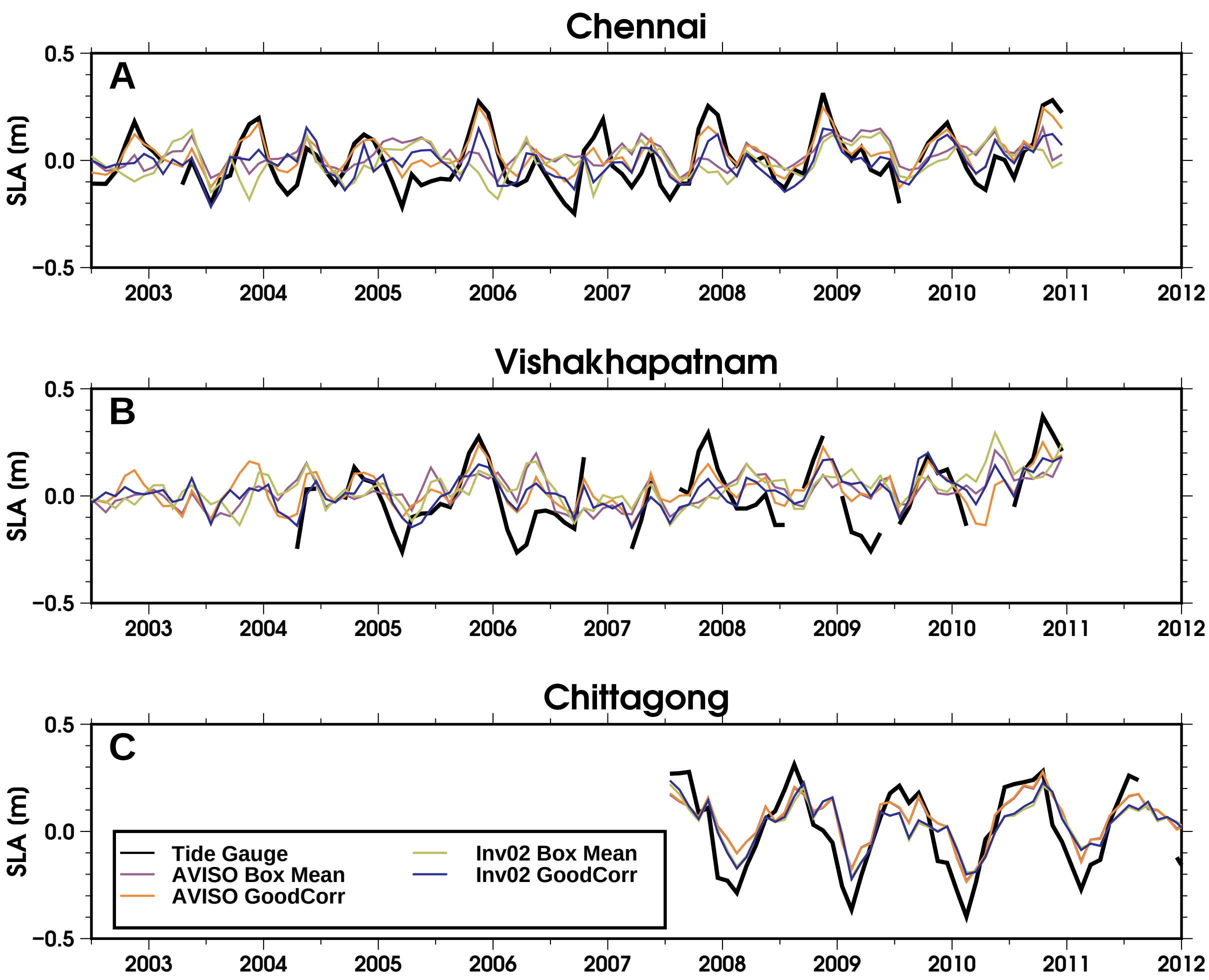

Figure 5. Comparison of TG time series. (A) Chennai TG, (B) Visakhapatnam TG, (C) Chittagong TG.

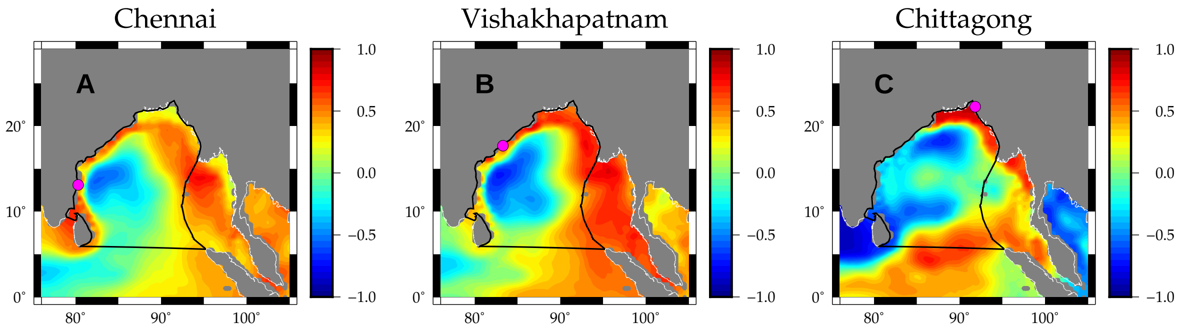

Figure 6. Correlation maps between the TGs (A) Chennai, (B) Visakhapatnam, (C) Chittagong and our inversion at each grid point.

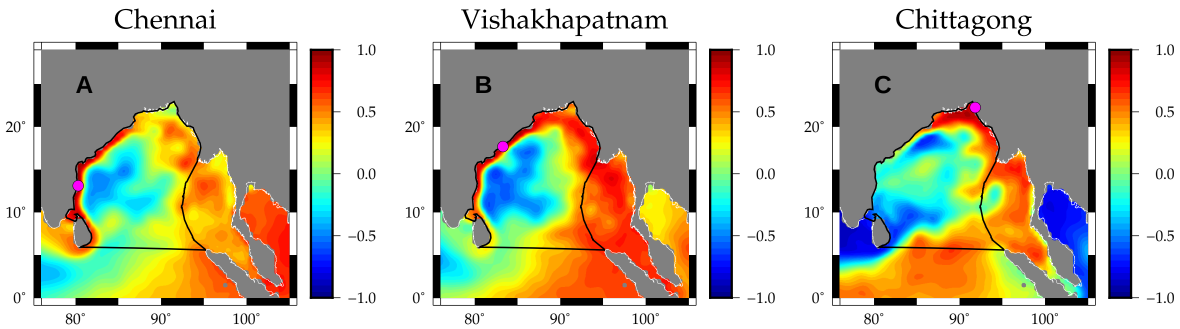

Figure 7. Correlation maps between the TGs (A) Chennai, (B) Visakhapatnam, (C) Chittagong and AVISO MSLA at each grid point.

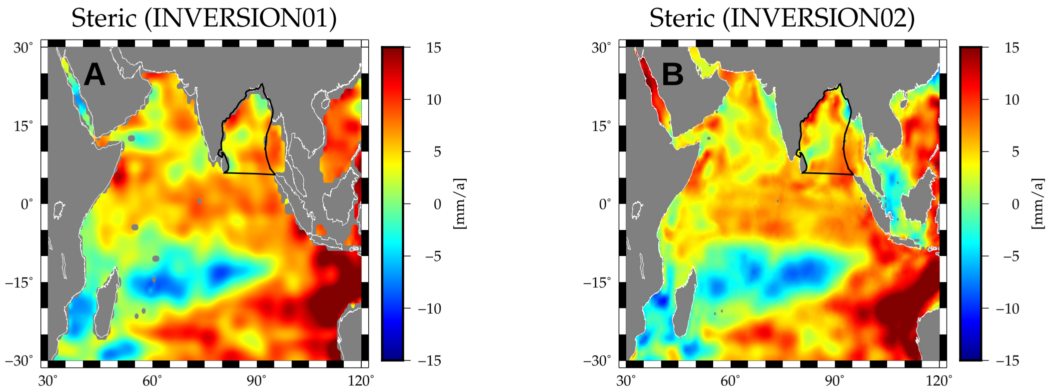

Figure 8. Total steric sea level (here derived as steric + residual) trend maps, 2004-2012, from the GRACE/altimetry inversion using FESOM- (INVERSION02) and Argo-based (INVERSION01) patterns, over the Indian Ocean. (A) INVERSION02. (B) INVERSION01.

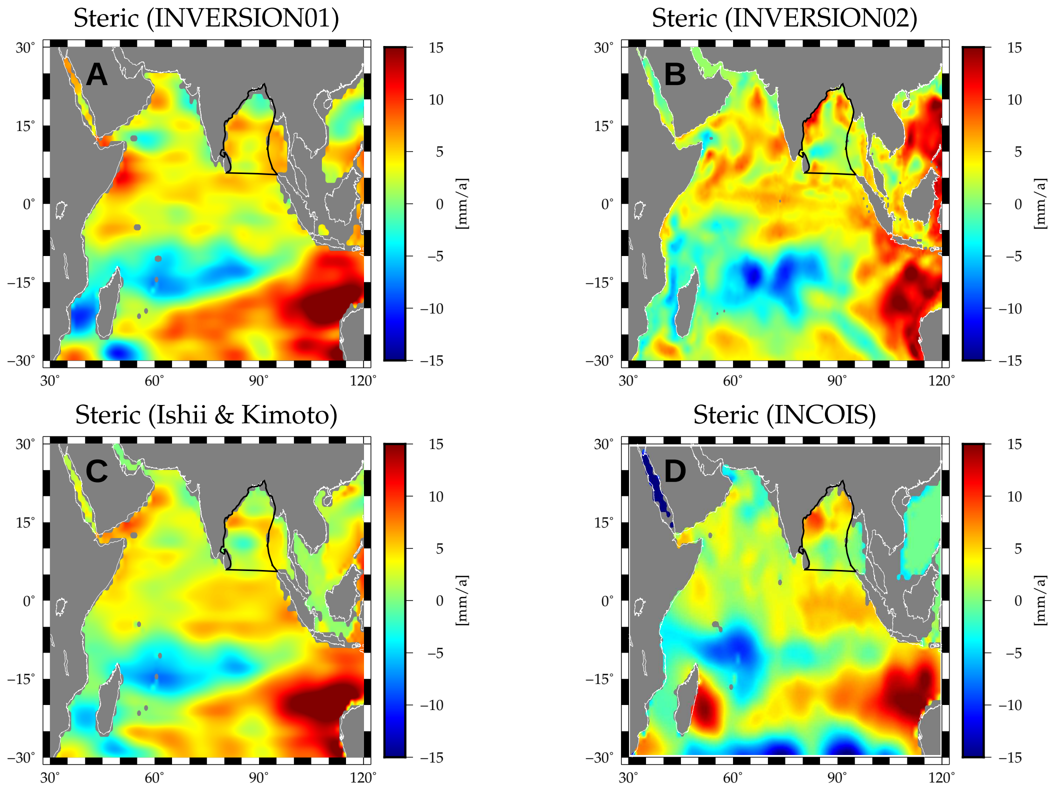

Figure 9. Steric sea level trends for the Indian Ocean, 2002-2012. (A) INVERSION02 (0m-seafloor). (B) INVERSION01 (upper 700 m). (C) INCOIS (upper 700 m). (D) Ishii and Kimoto (upper 700 m).

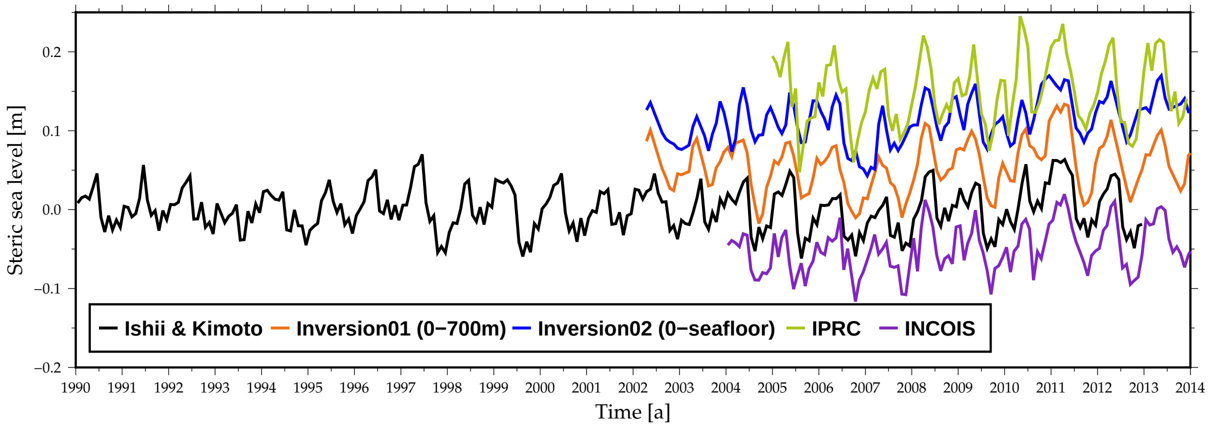

Figure 10. Steric sea level anomalies in the Bay of Bengal. Curves are plotted with an offset for clarity.

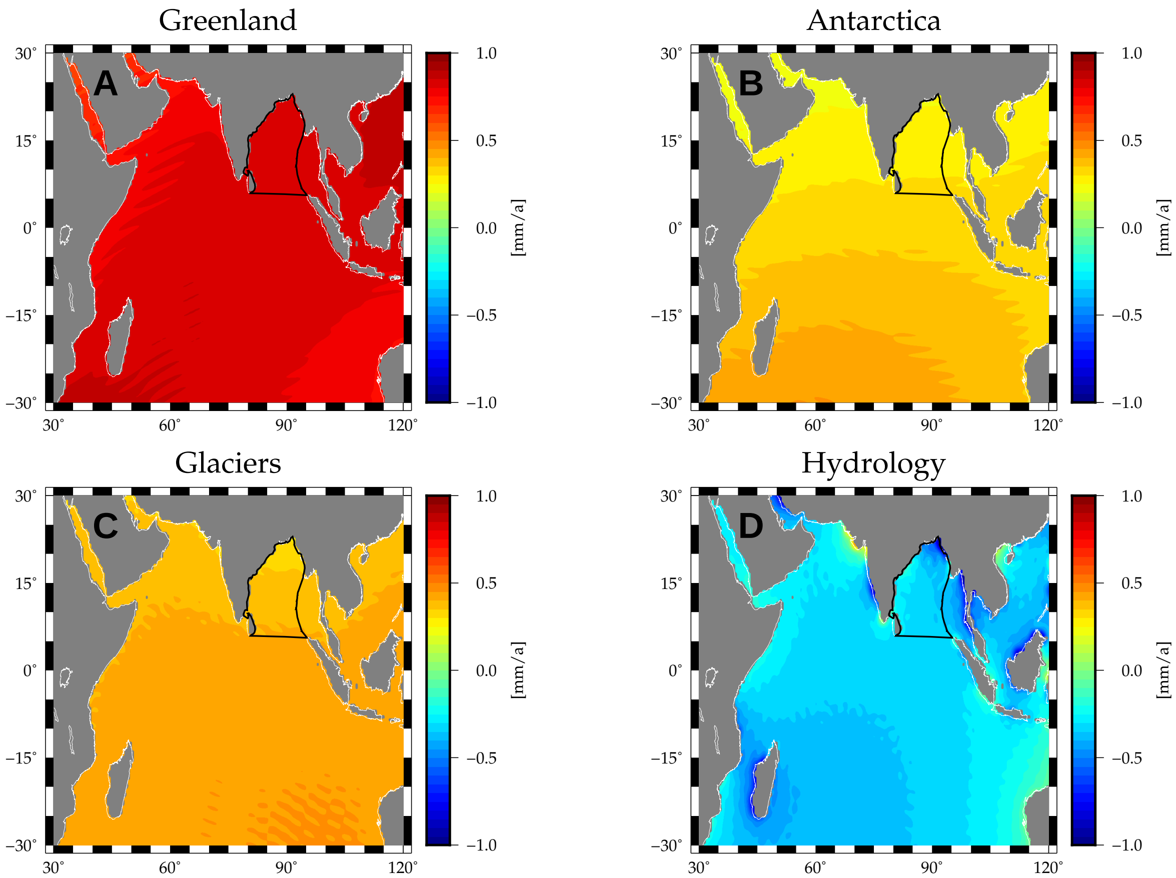

Figure 11. Mass contribution trends (2002-2014) to the total sea level. Top, left: Effect of Greenland mass loss. Top, right: Antarctica. Bottom, left: World glaciers. Bottom, right: Land hydrology.

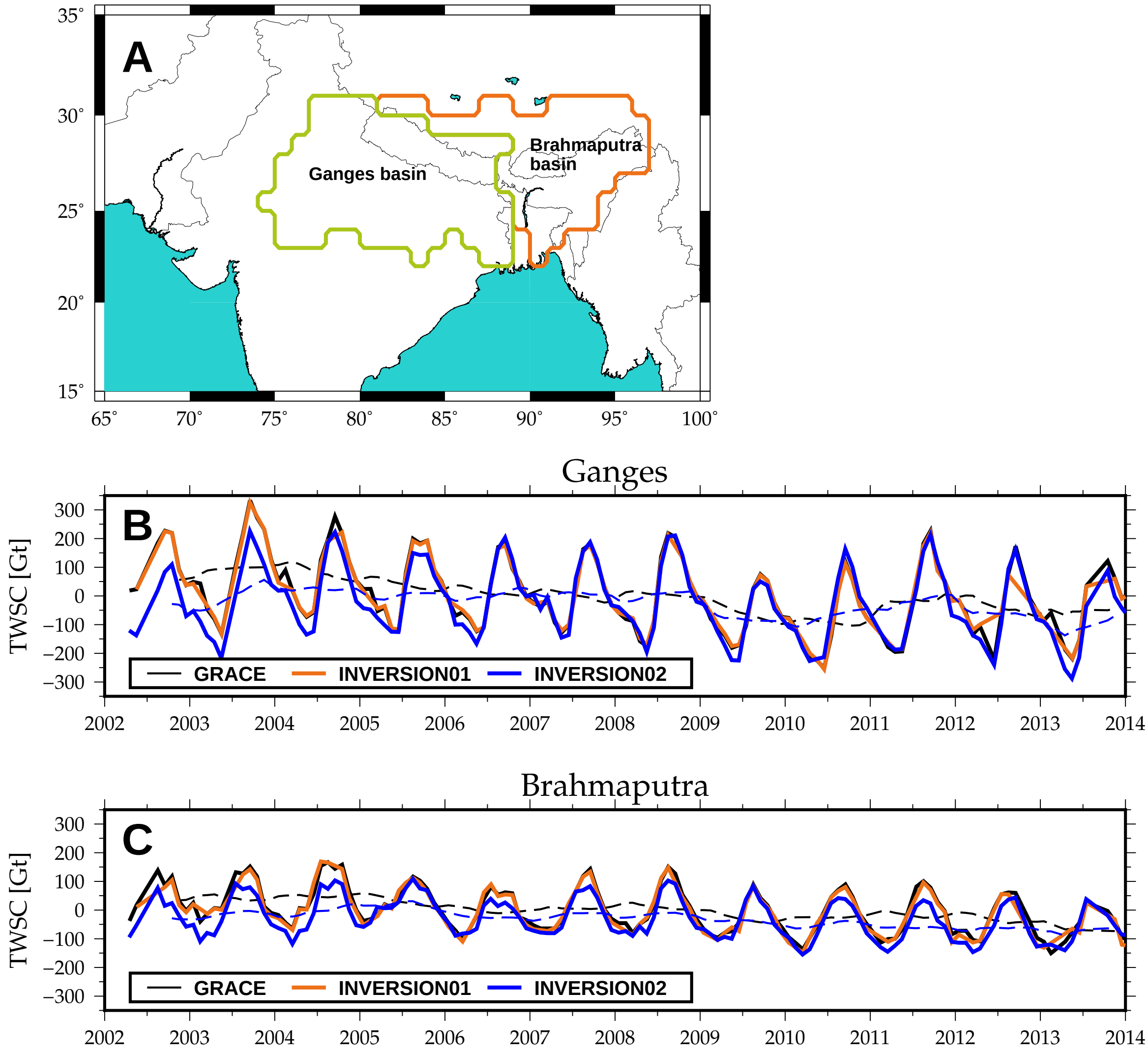

Figure 12. Basin averaging Total Water Storage Content (TWSC) results from GRACE and our inversion for the Ganges and Brahmaputra basin. (A) Map which shows the location of the basins. (B) TWSC in the Ganges basin from 2002 to 2014. (C) TWSC in the Brahmaputra basin from 2002 to 2014. The black and blue dashed lines represent the long periodic mass changes, filtered by a 12-month moving average, from GRACE and our inversion, respectively.

Table 3. Basin average trends (August 2002 - July 2009) in [Gt/a] from our inversion and GRACE (DDK3) compared to estimates from Jensen et al., 2013. The values in parenthesis in the GRACE column are taken from Jensen et al. (2013) and are based on RL04 GRACE solutions and a different rescaling approach.

Basin	GRACE	Inversion	Jensen et al. 2013
Ganges	-19.52 (-22.6)	-1.84	-18.1
Brahmaputra	-9.93 (-12.4)	-2.90	3.4

Table 4. Trends and accelerations for individual sea level components in the Bay of Bengal. The last column reports the change in absolute sea level in 2050 relative to 2005 utilizing the reported trends and accelerations.

Contribution	**Trend** $[\frac{mm}{a}]$	**Acceleration** $[\frac{mm}{a^2}]$	**SLC 2050 - 2005** $[m]$
Mass (GRACE+altimetry)	1.17 ± 0.06	0.0738 ± 0.0203	0.20
Antarctica	0.28 ± 0.02	0.0135 ± 0.0062	0.04
Greenland	0.84 ± 0.01	0.0331 ± 0.0026	0.10
Hydrology	-0.31 ± 0.05	0.0342 ± 0.0169	0.06
Glaciers	0.36 ± 0.02	-	0.02
Steric (CMIP5, MPI-M)			
RCP2.6	3.08 ± 0.70	-0.0353	0.07
RCP4.5	3.08 ± 0.70	0.0112	0.16
RCP8.5	3.08 ± 0.70	0.0261	0.19

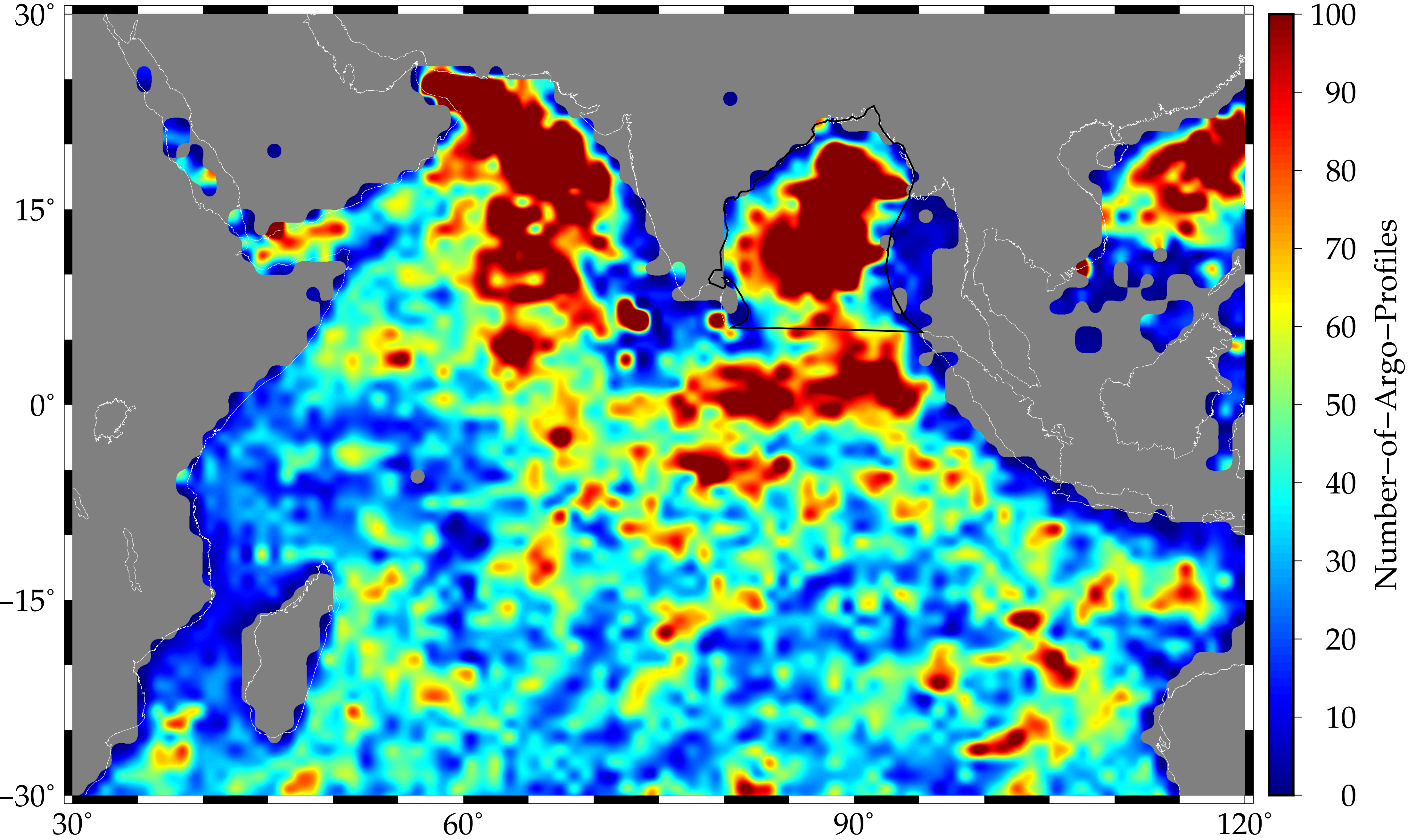
30°
15°
0°
−15°
−30°
30°
60°
90°
120°
100
90
80
70
60
50
40
30
20
10
0
Number−of−Argo−Profiles

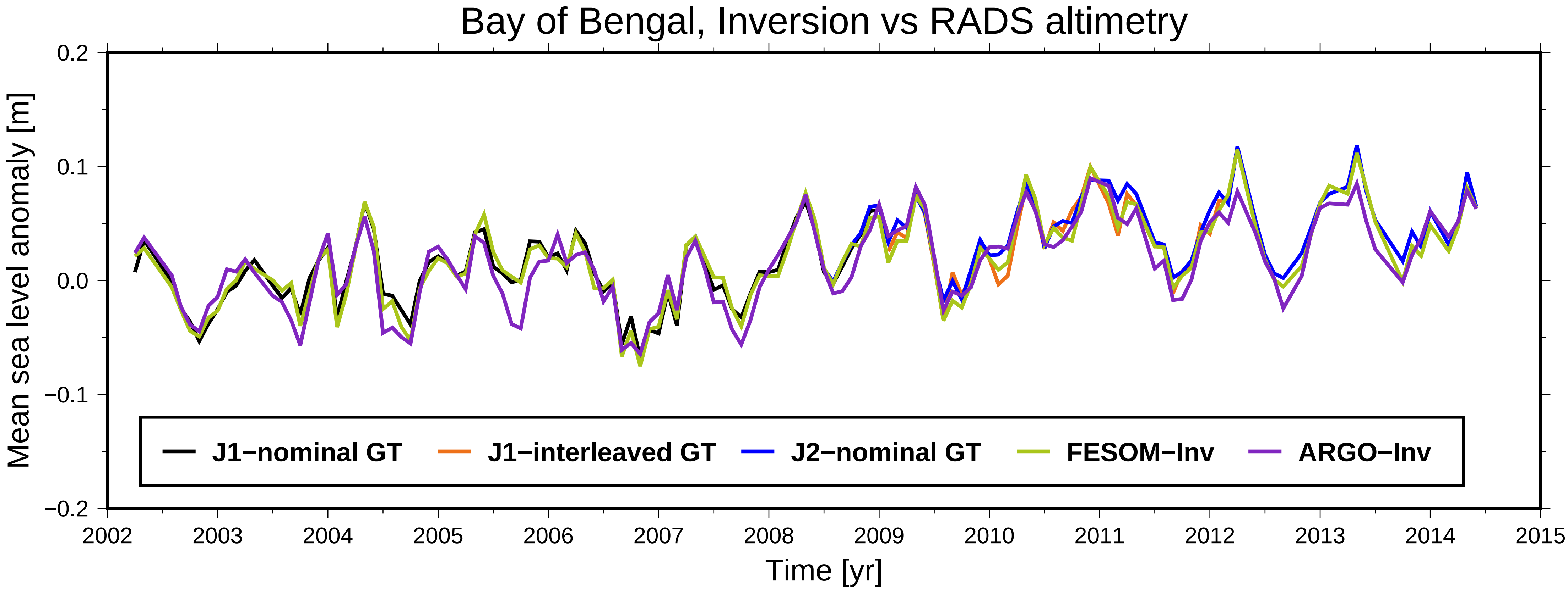

Bay of Bengal, Inversion vs RADS altimetry
Mean sea level anomaly [m]
0.2
0.1
0.0
−0.1
−0.2
2002
2003
2004
2005
2006
2007
2008
2009
2010
2011
2012
2013
2014
2015
Time [yr]
J1−nominal GT
J1−interleaved GT
J2−nominal GT
FESOM−Inv
ARGO−Inv

Bay of Bengal, Bin Locations

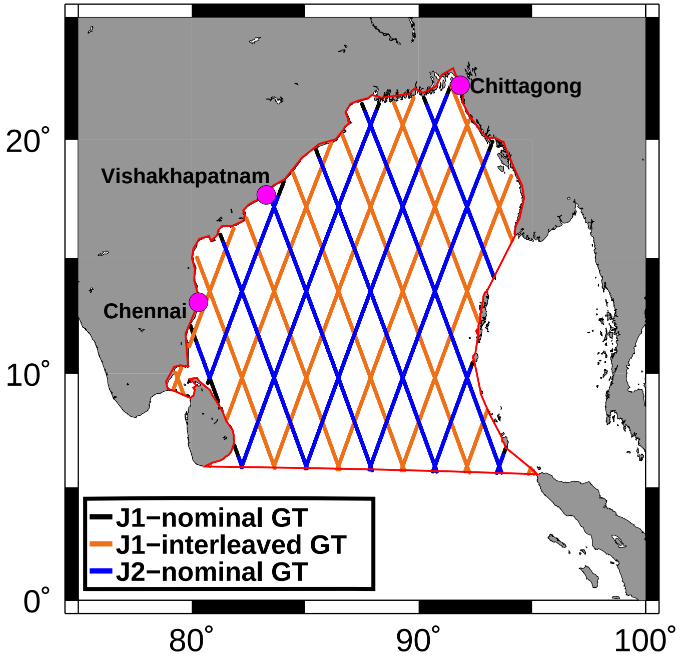

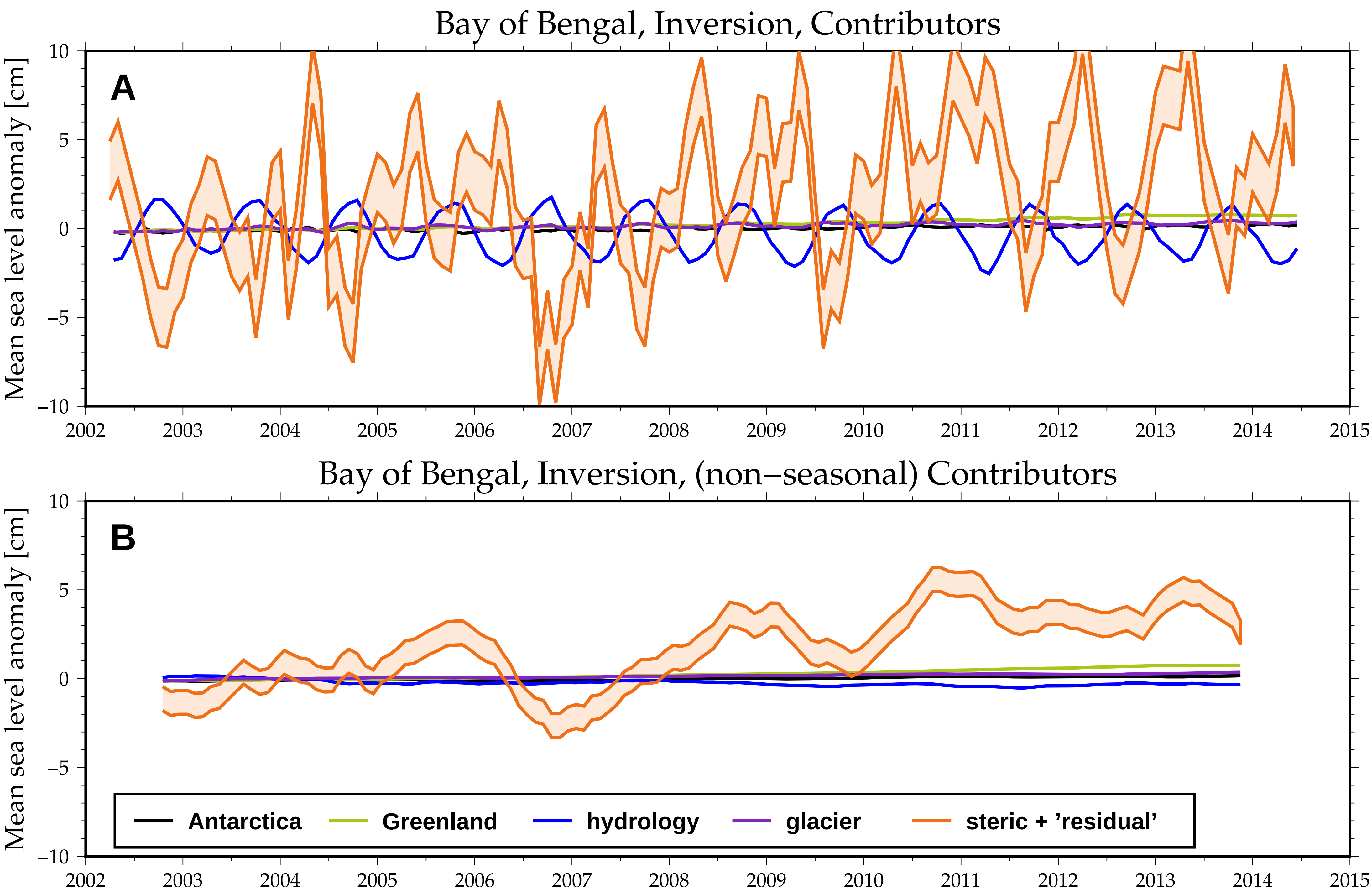
Bay of Bengal, Inversion, Contributors
A
Mean sea level anomaly [cm]
10
5
0
−5
−10
2002
2003
2004
2005
2006
2007
2008
2009
2010
2011
2012
2013
2014
2015
Bay of Bengal, Inversion, (non−seasonal) Contributors
B
Antarctica
Greenland
hydrology
glacier
steric + 'residual'

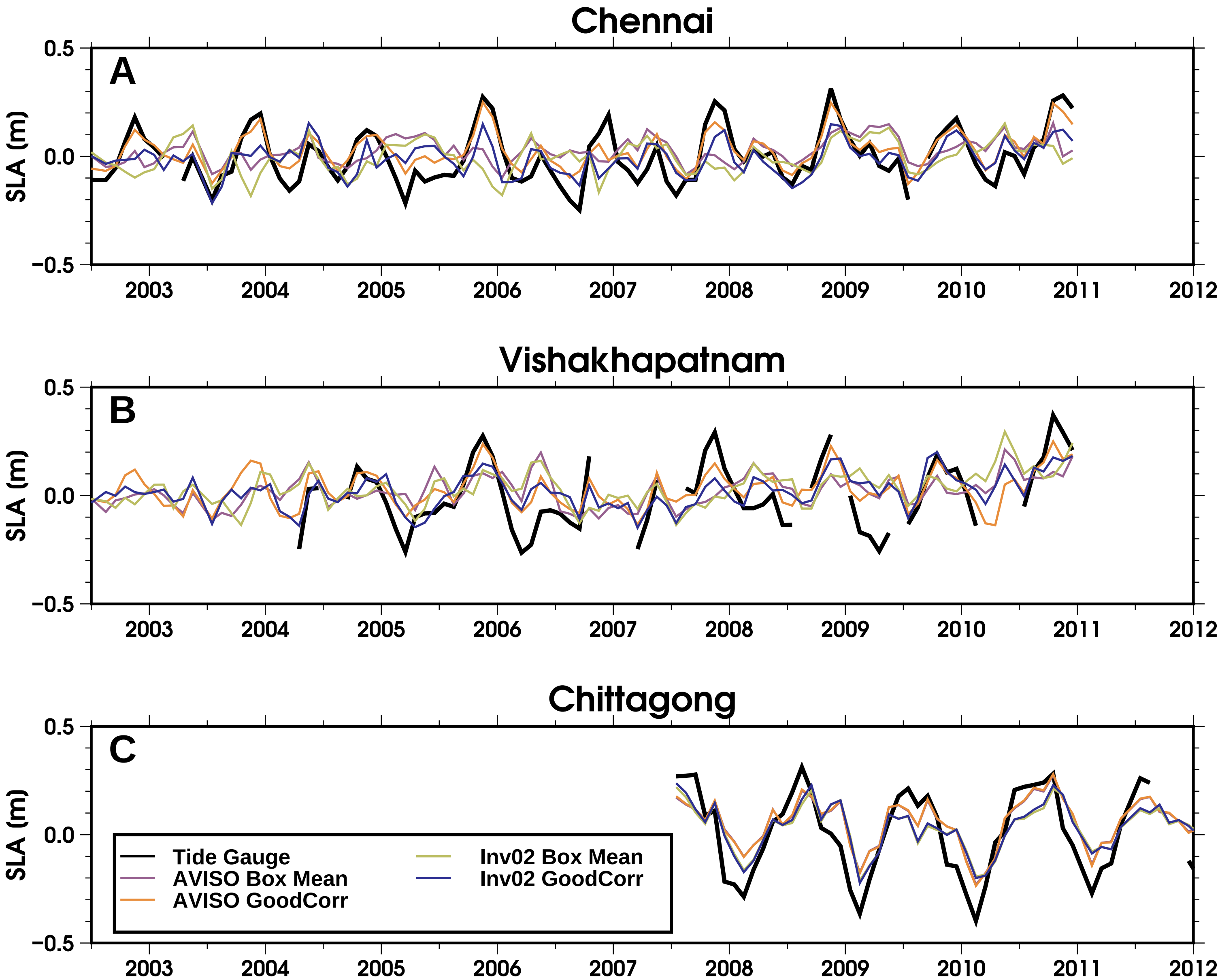
Chennai
A
SLA (m)
0.5
0.0
−0.5
2003
2004
2005
2006
2007
2008
2009
2010
2011
2012
Vishakhapatnam
B
SLA (m)
0.5
0.0
−0.5
2003
2004
2005
2006
2007
2008
2009
2010
2011
2012
Chittagong
C
SLA (m)
0.5
0.0
−0.5
Tide Gauge
AVISO Box Mean
AVISO GoodCorr
Inv02 Box Mean
Inv02 GoodCorr
2003
2004
2005
2006
2007
2008
2009
2010
2011
2012

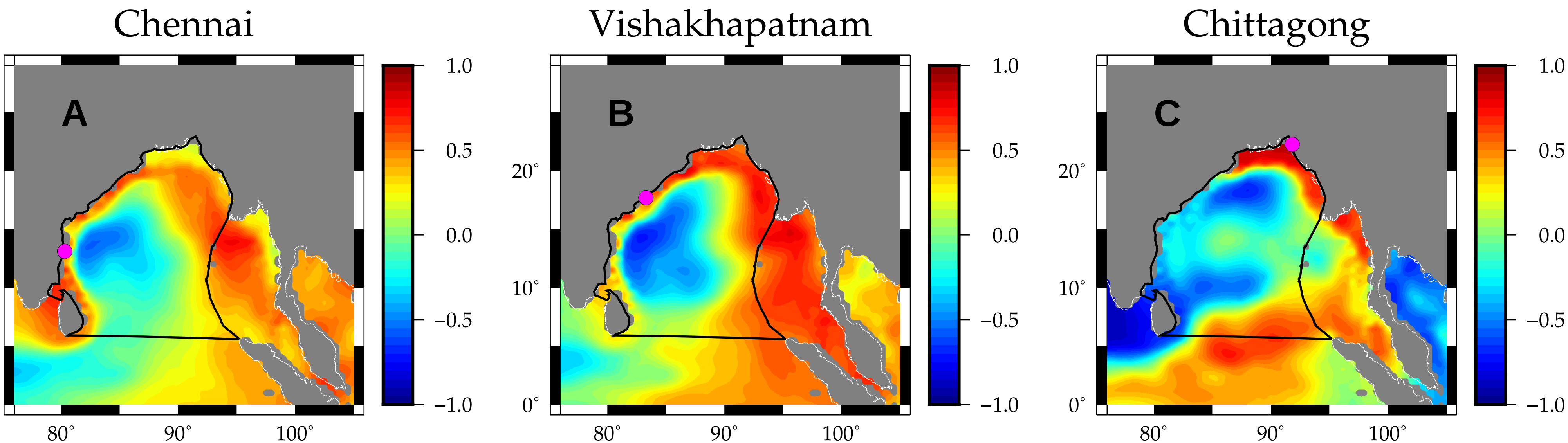
Chennai
Vishakhapatnam
Chittagong
A
B
C
1.0
0.5
0.0
−0.5
−1.0
20°
10°
0°
80°
90°
100°

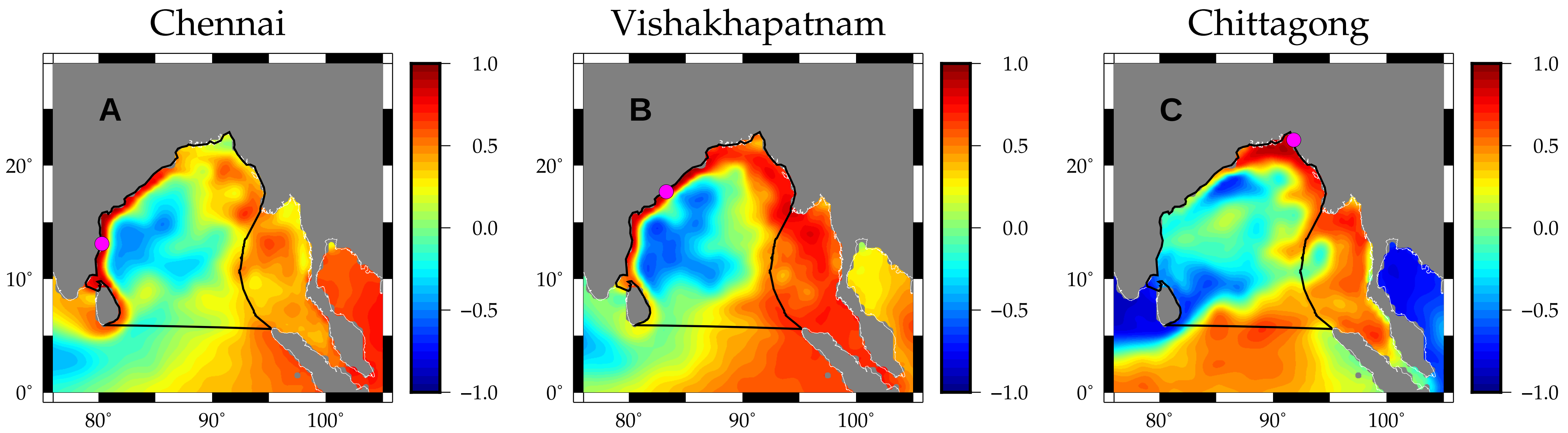

Chennai
Vishakhapatnam
Chittagong
A
B
C
20°
10°
0°
80°
90°
100°
1.0
0.5
0.0
−0.5
−1.0

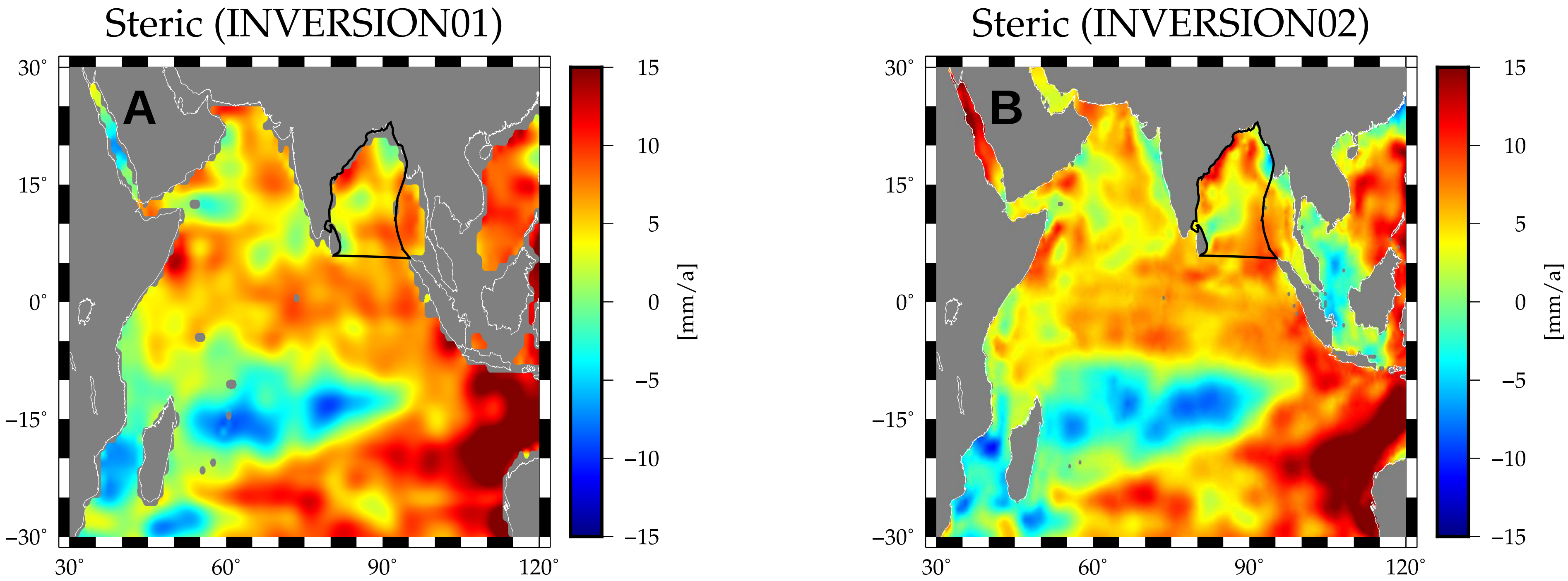

Steric (INVERSION01)
A
30°
15°
0°
−15°
−30°
30°
60°
90°
120°
15
10
5
0
−5
−10
−15
[mm/a]
Steric (INVERSION02)
B
30°
15°
0°
−15°
−30°
30°
60°
90°
120°
15
10
5
0
−5
−10
−15
[mm/a]

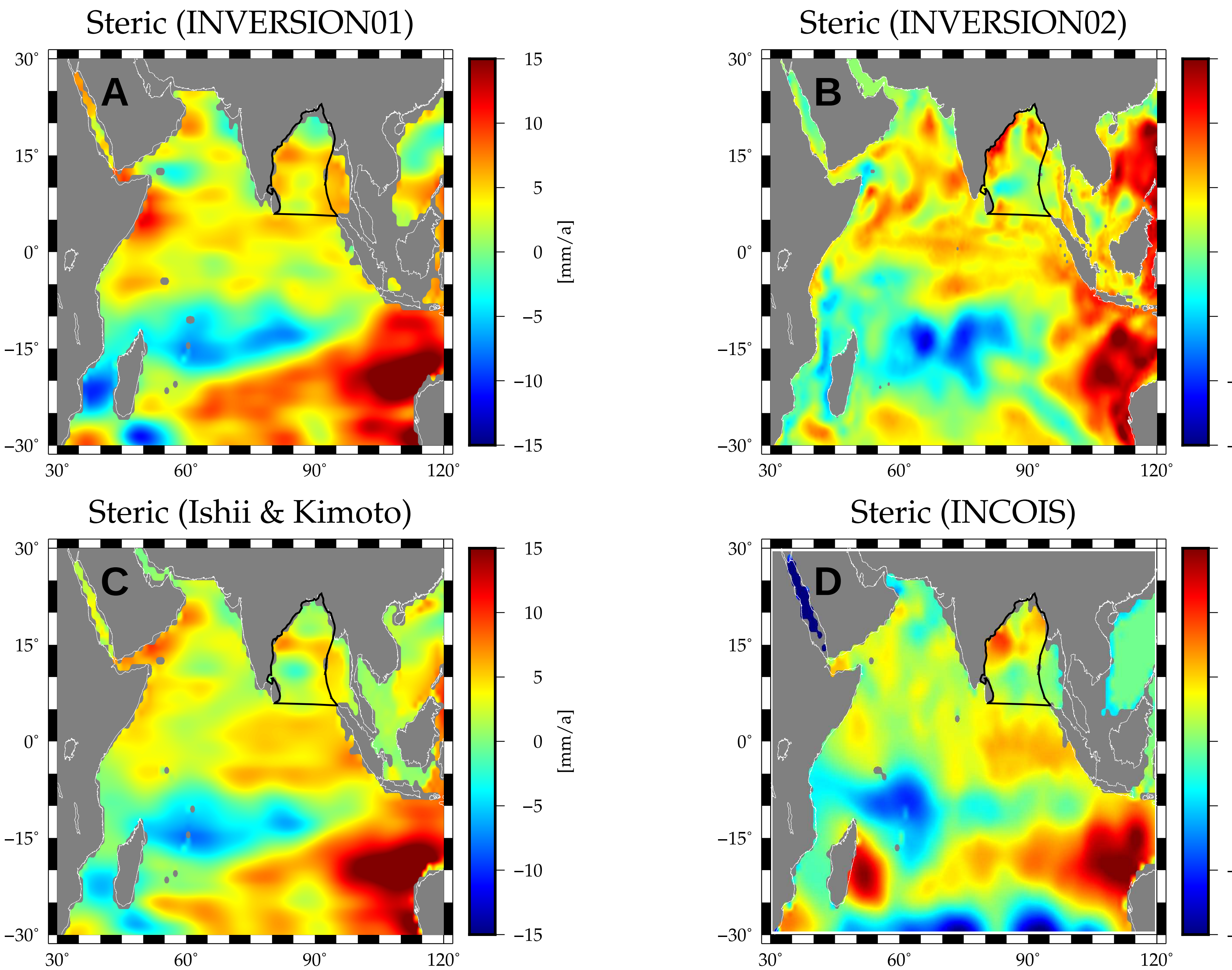

Steric (INVERSION01)
A
Steric (INVERSION02)
B
Steric (Ishii & Kimoto)
C
Steric (INCOIS)
D
30°
15°
0°
−15°
−30°
30°
60°
90°
120°
15
10
5
0
−5
−10
−15
[mm/a]

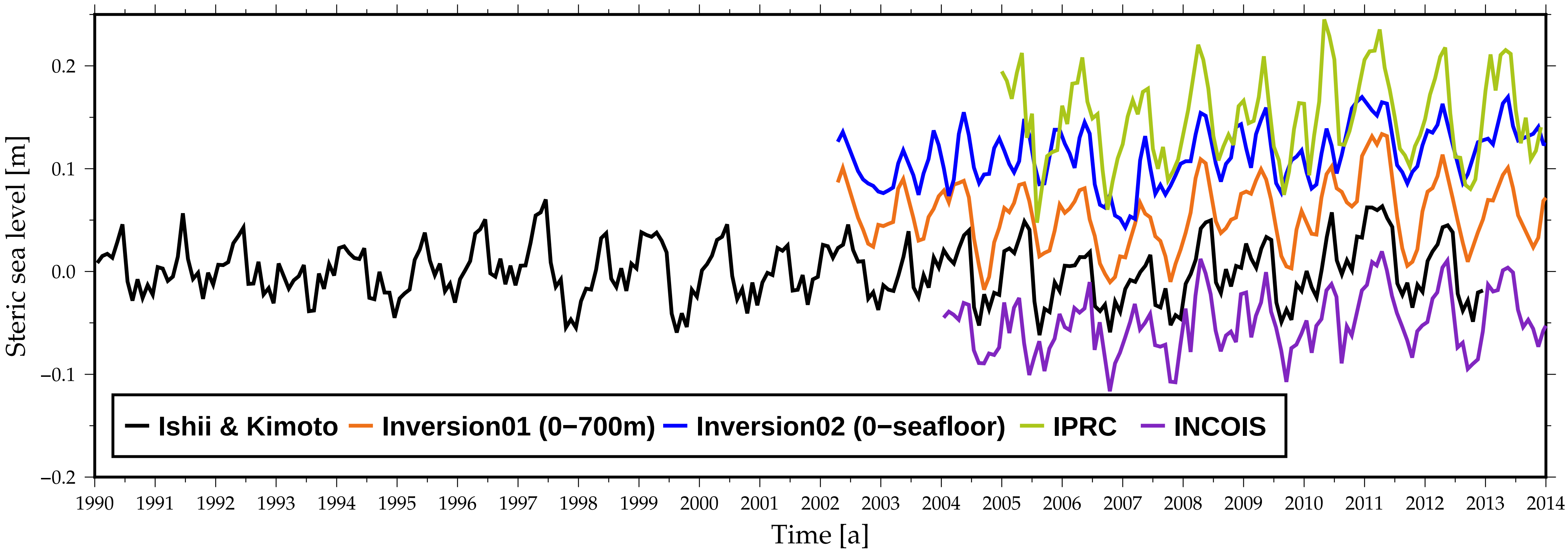

Steric sea level [m]
0.2
0.1
0.0
−0.1
−0.2
Ishii & Kimoto
Inversion01 (0−700m)
Inversion02 (0−seafloor)
IPRC
INCOIS
1990
1991
1992
1993
1994
1995
1996
1997
1998
1999
2000
2001
2002
2003
2004
2005
2006
2007
2008
2009
2010
2011
2012
2013
2014
Time [a]

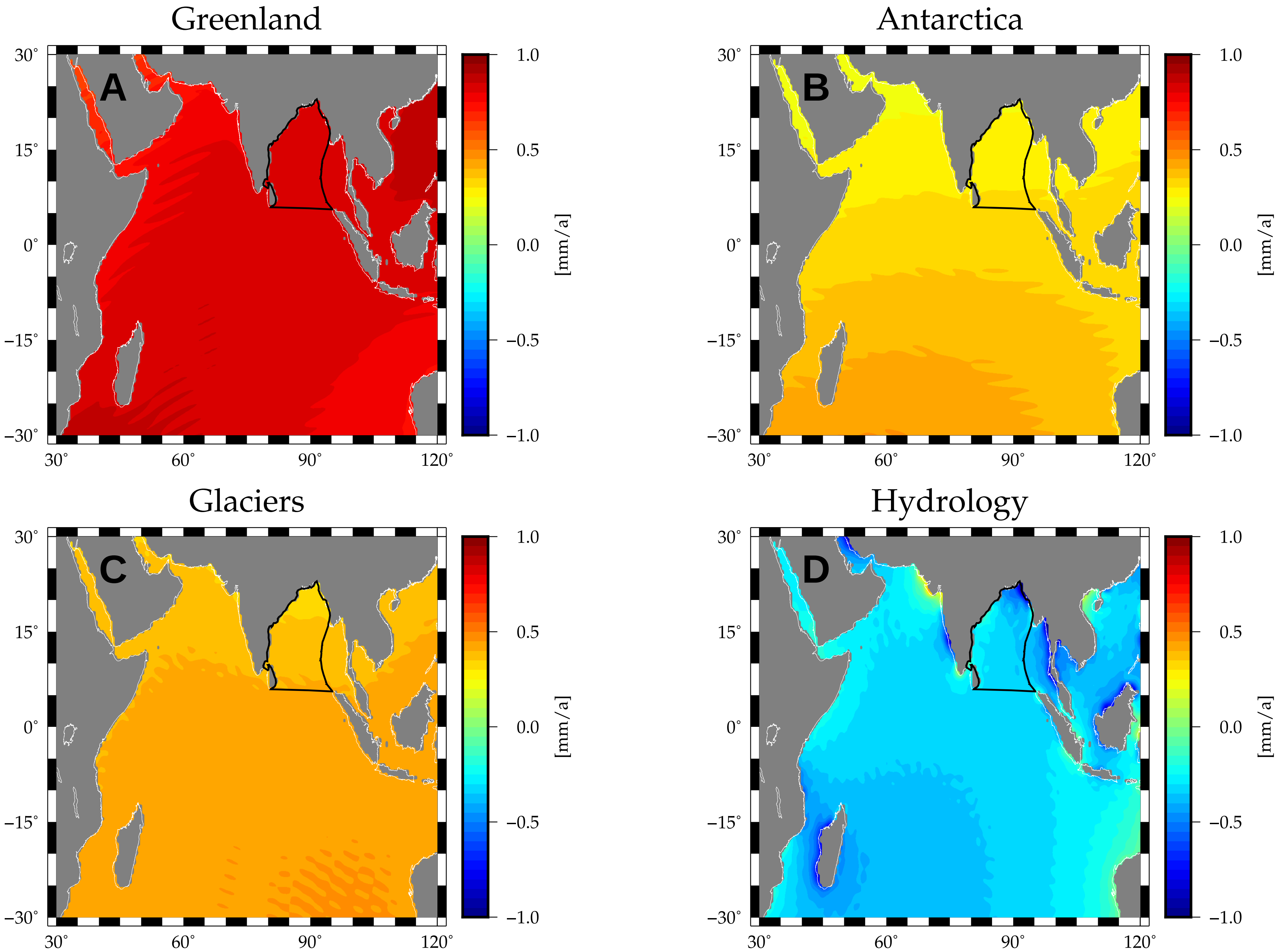

Greenland
Antarctica
Glaciers
Hydrology
A
B
C
D
30°
15°
0°
−15°
−30°
30°
60°
90°
120°
1.0
0.5
0.0
−0.5
−1.0
[mm/a]

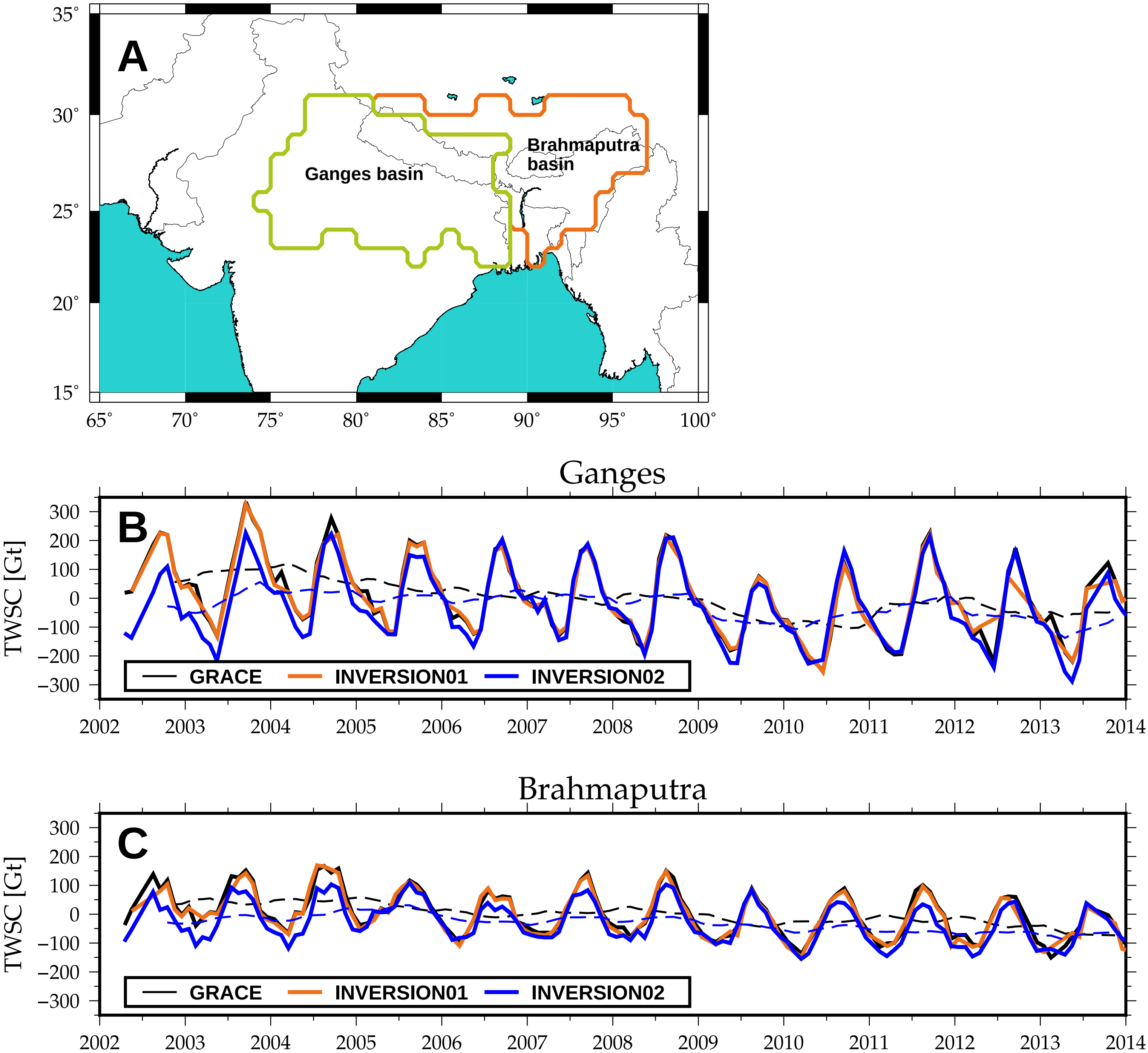
A
Ganges basin
Brahmaputra basin
35°
30°
25°
20°
15°
65°
70°
75°
80°
85°
90°
95°
100°
Ganges
B
TWSC [Gt]
GRACE
INVERSION01
INVERSION02
2002
2003
2004
2005
2006
2007
2008
2009
2010
2011
2012
2013
2014
Brahmaputra
C
TWSC [Gt]
GRACE
INVERSION01
INVERSION02